POLITEKNIK NEGERI BALI

Journal of Engineering Design and Technology

logic

Vol.19 No.3 November 2019

LOGIC

Jurnal Rancang Bangun dan Teknologi

p-ISSN. 1412-114X

e-ISSN. 2580-5649

LOGIC

Jurnal Rancang Bangun dan Teknologi

Journal of Engineering Design and Technology

Gedung P3M, lt.1 Politeknik Negeri Bali, Bukit Jimbaran
PO BOX 1064 Kuta Selatan, Badung, Bali - Indonesia
Telp. (+62)361 701981 Fax. (+62)361 701128
Email: logic@pnb.ac.id

LOGIC JOURNAL TEAM

PREFACE

Logic: Jurnal Rancang Bangun dan Teknologi (Journal of Engineering Design and Technology) is a peer-reviewed research journal aiming at promoting and publishing original high quality research in all disciplines of engineering and applied technology. All research articles submitted to Logic should be original in nature, never previously published in any journal or presented in a conference or undergoing such process across the world. All the submissions will be peer-reviewed by the panel of experts associated with particular field. Submitted papers should meet the internationally accepted criteria and manuscripts should follow the style of the journal for the purpose of both reviewing and editing.

Logic is a journal covering articles in the field of civil and mechanical engineering, design, and technology published 3 times a year in March, July, and November. Language used in this journal is English.

LOGIC. P-ISSN 1412-114X
LOGIC. E-ISSN 2580-5649
Indexing : GOOGLE SCHOLAR, DOAJ, EBSCO OPEN SCIENCE DIRECTORY, SINTA 3

Best Regard,

LOGIC Editorial Team

TABLE OF CONTENTS

LOGIC
Journal of Engineering Design and Technology
Vol. 19 No.3 November 2019; p. 107 - 114

p-ISSN : 1412-114X
e-ISSN : 2580-5649
http://ojs.pnb.ac.id/index.php/LOGIC

THE EVALUATION OF BULUSAN LANDFILL CAPACITY IN BANYUWANGI

Abdul Holik[*)1], Zulis Erwanto [*)], Mohammad Aziz Yusuf [*)]

*) Politeknik Negeri Banyuwangi, Jl. Raya Jember Km. 13 labanasem Kabat Banyuwangi.

Correponding email [1)] : abdulholik@poliwangi.ac.id

Abstract. *The Bulusan landfill of Banyuwangi has 1.5 ha to accommodate garbage from 13 districts with an input of 451.8 m^3 of garbage per day and controlled landfill methods are carried out as garbage management. This research aims to evaluate the capacity of the Bulusan Landfill in Banyuwangi. Arithmetic, geometric and least square method were selected by the highest correlation value. The projection result of the Bulusan landfill for 2018 has been declared overloaded, with the height of embankment was higher than the planned embankment and it has not been able to accommodate garbage. The projection for the next 15 years from 2017 to 2031 was predicted that Bulusan landfill will be overloaded at 1.172.185 m^3 of garbage volume. Financial and technical feasibility studies for candidates for the Bulusan landfill replacement need to be carried out so that the Bulusan landfill replacement project can be realized immediately.*

Keywords: Carrying Capacity, Landfill, Over Load, R square

1. INTRODUCTION

Solid garbage is consisting of organic materials and inorganic materials which are considered useless and must be managed so as not to endanger the environment and protect development investment. Solid garbage as a result of various activities in human life and the results of a natural process often cause serious problems in residential areas. With the increase in population, it will certainly produce garbage products that must be faced by the area and reduced land for processing garbage.

according to [1] The landfill generated from a city can be obtained by surveying measurements or direct analysis in the field with; Measuring directly the generation of garbage units from a number of samples (household and non-household) determined randomly at source for 8 consecutive days (SNI 19-3964-1995 and SNI M 36-1991-03), Measuring the amount (weight and / or volume) of garbage entering the TPS, High-volume analysis, and balance analysis material.

Research on handling landfills has been carried out, [2] predicting and analyzing landfills in the city of Padang, [3] evaluating domestic solid garbage management systems in Palembang. Whereas the determination of landfill is assessed by [4] wherein estimating the availability of landfills, data mining and linear regression algorithms are used. While [5] applies the Weight Aggregated Sum-Product Assessment (WASPAS) method and the Multi-Objective Optimization On Base of Ratio Analysis (MOORA) method to determine the landfill Site in Medan City.

Although the new landfill plan can be predicted, it is still necessary to estimate the projected capacity of the Bulusan landfill by determining the remaining capacity of the Bulusan landfill. To calculate cell landfill capacity, landfill planning dimension data is needed such as cell column length, cell pool width, cell pool bottom width, cell pool depth, cell pool edge slope, and cell pool base slope. Whereas for the process of analyzing land capacity and needs, it is necessary to calculate the area, planned depth/thickness, the generation rate of garbage generation, the density of garbage before compacting and after solidification, and the percentage of volume reduction after solidification.

2. METHODS

2.1. Data Collection

data consists of primary data and secondary data. The primary data is landfill dimension and the secondary data are the amount of garbage per year, landfill plan age, landfill area, facilities, infrastructure in landfill, the population of 13 sub-districts in Banyuwangi Regency from 2006 – 2016 which collected from Dinas Lingkungan Hidup (DLH) and Badan Pusat Statistik (BPS) of Banyuwangi.

2.2. Correlation Coefficient

The Correlation Coefficient (Eq.1) is used to find out the relationship between two variables (population and amount of garbage) and know how the relationship is going. This correlation aims to determine the three extrapolation methods (Arithmetic, Geometric and Least square methods), which method is suitable for calculating population projections and the amount of garbage.

$$r = \frac{n \sum x y - \sum x \sum y}{\sqrt{\{n \sum x^2 - (\sum x)^2\}\{n \sum y^2 - (\sum y)^2\}}} \quad (1)$$

Where r is correlation coefficient value, x is the first variable value, y is a second variable value, and n is an amount of data.

2.3. Arithmetic Method

The Arithmetic Method (Eq.2) is generally used if the population growth is relatively constant each year. The equation used is:

$$p_{n=} p_{o+R.n} \quad (2)$$

Where p_n is the number of population in a year, p_o is the initial population, R is the amount of population growth each year, and n is the number of years projected.

2.4. Geometric Method

The Geometric Method (Eq.3) is generally used if the population growth rate rises multiple or the population growth rate changes equivalent to the previous year's population. The equation used is:

$$p_{n=} p_{o\,(1+r)^n} \quad (3)$$

Where $p_n$is number of population in a year, p_o is initial population, r is a percentage of population growth each year, and n is the number of years projected.

2.5. Least Square Method

The Least Square Method (Eq.4) is used if the data regression line of past population development describes linear line trends, although population growth does not always increase. The equation used is:

$$y = A + \quad B._x \quad (4)$$

$$A = \frac{(\sum Y_i)(\sum X_i^2) - (\sum X_i)(\sum X_i \quad Y_i)}{n \sum x_1^2 - (\sum x_1)^2} \quad (5)$$

$$B = \frac{n \quad \sum X_i \quad Y_i \quad - \quad (\sum X_i) \quad (\sum Y_i)}{n \sum x_1^2 - (\sum x_1)^2} \quad (6)$$

Where y is total population, x is an additional amount of base year, $A, B$are Constants, and n is the amount of data.

2.6. Landfill capacity

The data required for Calculating cell landfill capacity are cell column length, cell pool width, cell pool bottom width, cell pool depth, cell pool edge slope, cell pool base slope. Landfill cells can be a parallelogram, triangle and trapezoidal shapes. To calculate the capacity of a cell landfill, the formula is used:

$$V = (a \times t) \times p \quad (7)$$

$$V = (0{,}5 \times la \times t) \times p \quad (8)$$

$$V = la + lb \times t \times p \quad (9)$$

$$Total\ volume = n \times v \quad (10)$$

Where *V* is volume of *cell landfill* (m³), *la* is wide up of *cell landfill* (m), *lb* is bottom width of *cell landfill* (m), *t* is depth of *cell landfill* (m), *p* is length of *cell landfill* (m), and *n* is lots of *cell landfill*.

2.7. Analysis of Land needs and capacity

The requirements according to the Ministry of Public Works (1995) as follows: Location area, Planned depth/thickness of the layer, Garbage generation rate, Density of garbage before compacting and after compacting, and Percentage of volume reduction after compacting. Calculation of land requirements for Sanitary Landfill uses the following formula:

$$V = \frac{R}{D}\left(1 - \frac{P}{100}\right) - C_v \quad (11)$$

$$V = \frac{V_N}{d} \quad (12)$$

Where V is a volume of solid garbage and overburden (m³/person/year), R is garbage generation rate per person per year (kg/person/year), The value of the rate of garbage generation is obtained from the amount of generation based on the classification of cities. D is density before solidified garbage that arrives at the landfill (kg / m³), the density value is obtained from the results of the assumptions of the determination of municipal garbage generation rates in Indonesia, (200 - 300 kg / m³). P is the percentage of volume reduction due to compaction with the tool (3 × trajectory) approximately 50% to 75% (provision). Cv is cover volume (m² / person / year). A is land area needed (m² / year), N is the number of population served, and d is high solid garbage and overburden.

Compaction ratio and calculation of land requirements of the landfill (Eq.13) is a reduction in the volume of garbage after undergoing a compaction process at the landfill. The assumption ratio of 1 part of overburden is compared to 4 parts of garbage (1: 4) with the formula:

$$V = 1{,}25 \quad \frac{R}{D} \quad \left(1 - \frac{P}{100}\right) \quad (13)$$

3. RESULTS AND DISCUSSION

3.1. Amount of Garbage and Total Population

Bulusan landfill is located at Bulusan village, Kalipuro district, Banyuwangi regency. Founded in 1986, effective use in 1988 and re-inaugurated after the renewal of names in 2012. The landfill has 1.5 ha of land area with 15 years of economic age. The amount of garbage entering bulusan's landfill in 2006-2013 was a relatively small increase. While the biggest increase was in 2014 (46.28%). In detail, the amount of garbage entering each year is presented in Table 1, while the increase and decrease in the amount of garbage can be seen in Figure 1.

Table 1. The amount of garbage entered in Bulusan landfill

No	Year	amount of garbage (m³)	garbage growth rate (m³)	the rate of garbage (%)
1	2006	27.621	5171	18,72
2	2007	32.792	(2359)	-7,19
3	2008	30.433	2619	8,61
4	2009	33.052	(406)	-1,23
5	2010	32.646	(3475)	-10,64
6	2011	29.171	1442	4,94
7	2012	30.613	267	0,87
8	2013	30.880	14292	46,28
9	2014	45.172	(1088)	-2,41
10	2015	44.084	440	1,00
11	2016	44.524	-	-
Total		380.988	16.903	58,95
Average		34.635	1.690	5,89

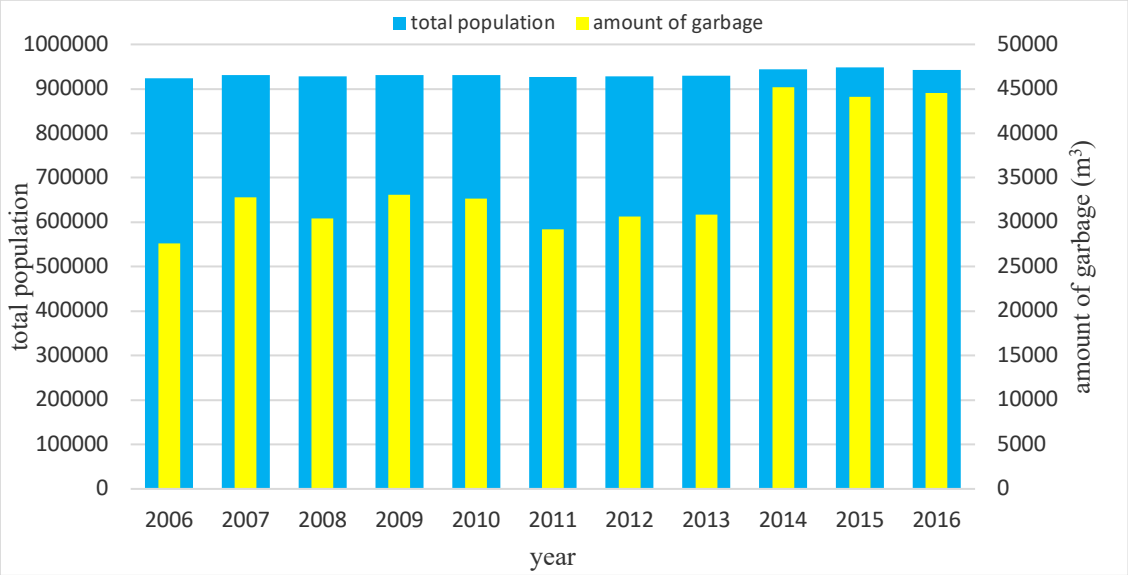

Figure 1. Graph of Population Growth and Garbage Rate (Analysis Results, 2018)

The Growth of population in 13 sub-districts showed a significant increase. The largest population is in 2015 with a population of 948,231. From 2006 to 2016, population growth increased by 1.98% or 18,257. From the calculation results, the average population growth is 932,881, the average percentage of population growth is 0.20% and the average amount of garbage is 34,635 m^3/day. The following is a recapitulation of population data from 13 sub-districts of Banyuwangi Regency as in Table 2.

Table 2. The population of 13 districts and Bulusan landfill garbage

No	year	Total population	Growth Total population	Population Growth (%)	Amount of garbage (m^3/day)
1	2006	924.171	6.409	0,69	27.621
2	2007	930.580	(2.924)	-0,31	32.792
3	2008	927.656	3.246	0,35	30.433
4	2009	930.902	(503)	-0,05	33.052
5	2010	930.399	(4.307)	-0,46	32.646
6	2011	926.092	1.787	0,19	29.171
7	2012	927.879	1.793	0,19	30.613
8	2013	929.672	14.014	1,51	30.880
9	2014	943.686	4.545	0,48	45.172
10	2015	948.231	(5.803)	-0,61	44.084
11	2016	942.428	-	-	44.524
Total		10.261.696	18.257	1,98	380.988
Average		932.881	1.826	0,20	34.635

The relationship between population and the amount of garbage each year shows a very strong, consistent and reliable correlation (R^2 = 0.9585). That is, the greater the increase in population, the greater the addition of garbage entering the Bulusan landfill. This correlation can be seen in Figure 2.

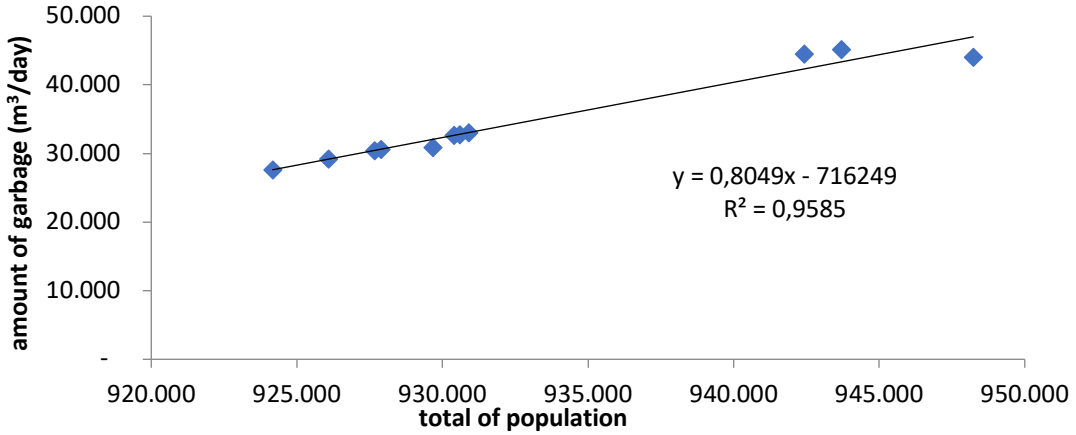

Figure 2. The coefficient of Correlation of Total Population with Amount of Garbage (Analysis Results, 2018)

3.2. Determination of The Correlation Method

This correlation aims to determine the three extrapolation methods (Arithmetic, Geometric and Least square methods) which are suitable to be used to calculate population projections and the amount of garbage. Determination of the method is obtained from the highest R^2 value. The results of the correlation calculation state that the suitable method used are the Geometric Method because it has the best correlation coefficient r among the three methods (Table 3). Furthermore, the data can be used as data to determine the projected population and the amount of garbage.

Table 3. Correlation results of various methods

Population Correlation Coefficient		The correlation coefficient of garbage	
Method	R^2	Method	R^2
Arithmetic	0,0008	Arithmetic	0,0131
Geometric	0,5941	Geometric	0,5827
Least Square	0,5431	Least Square	0,5292

3.3. Projection of Total Population and Amount of Garbage

To project the total population and the amount of garbage for the next 15 years in 13 districts, the geometric method was chosen. The projection of the total population in 2031 is 970,744 and amount of garbage is 105.125 m^3. This can be seen in Table 4 and Table 5.

Table 4. Projections of Total Population

year	Planning period	Least Square Constant		Projection of Total Population		
		$A=\frac{(\sum Y_i)(\sum X_i^2)-(\sum X_i)(\sum X_i Y_i)}{n\sum x_1^2-(\sum x_1)^2}$	$B=\frac{n\sum X_i Y_i-(\sum X_i)(\sum Y_i)}{n\sum x_1^2-(\sum x_1)^2}$	Least Square	Geometric	Arithmetic
	n			$Pn=(A+B.x)$	$Pn=Po(1+r)^n$	$Pn=(Po+R.n)$
2017	1	923,280	1,904	925,184	944,290	944,254
2018	2	923,280	1,904	927,088	946,155	946,079
2019	3	923,280	1,904	928,992	948,024	947,905
2020	4	923,280	1,904	930,896	949,897	949,731
2021	5	923,280	1,904	932,800	951,774	951,556
2022	6	923,280	1,904	934,705	953,654	953,382
2023	7	923,280	1,904	936,609	955,538	955,208
2024	8	923,280	1,904	938,513	957,425	957,034
2025	9	923,280	1,904	940,417	959,317	958,859
2026	10	923,280	1,904	942,321	961,212	960,685
2027	11	923,280	1,904	944,225	963,111	962,511
2028	12	923,280	1,904	946,129	965,013	964,336
2029	13	923,280	1,904	948,034	966,920	966,162
2030	14	923,280	1,904	949,938	968,830	967,988
2031	15	923,280	1,904	951,842	970,744	969,813

Table 5. Projection Amount of Garbage

year	Planning period	Least Square Constant		Projection Amount of Garbage (m^3)		
		$A=\frac{(\sum Y_i)(\sum X_i^2)-(\sum X_i)(\sum X_i \ Y_i)}{n\sum x_1^2-(\sum x_1)^2}$	$B=\frac{n \ \sum X_i \ Y_i \ - \ (\sum X_i) \ (\sum Y_i)}{n\sum x_1^2-(\sum x_1)^2}$	Least Square	Geometric	Arithmetic
	n			$Pn=(A+B.x)$	$Pn=Po(1+r)^n$	$Pn=(Po+R.n)$
2017	1	26.740	1.563	28.304	47.149	44.530
2018	2	26.740	1.563	28.305	49.928	44.536
2019	3	26.740	1.563	28.306	52.871	44.542
2020	4	26.740	1.563	28.307	55.987	44.548
2021	5	26.740	1.563	28.308	59.288	44.553
2022	6	26.740	1.563	28.309	62.783	44.559
2023	7	26.740	1.563	28.310	66.483	44.565
2024	8	26.740	1.563	28.311	70.402	44.571
2025	9	26.740	1.563	28.312	74.552	44.577
2026	10	26.740	1.563	28.313	78.947	44.583
2027	11	26.740	1.563	28.314	83.601	44.589
2028	12	26.740	1.563	28.315	88.529	44.595
2029	13	26.740	1.563	28.316	93.747	44.601
2030	14	26.740	1.563	28.317	99.273	44.607
2031	15	26.740	1.563	28.318	105.125	44.612

3.4. Landfill Capacity

It was Known that;

Landfill land area = 9.514 m^2
The height of plan pile = 15 m
Age of plan = 15 years
Solid factor = 2.5
So, the Capacity = 9.514 m^2 x 15 m^2= 142,710 m^3

3.5. Capacity Effectiveness of Machinery

The machinery owned by Bulusan landfill includes 1 excavator, 1 bulldozer and 1 loader. The loader is still in the repair stage so it cannot be operated. The volume of garbage entering the Bulusan Landfill on average each month is ± 3987.1 m^3, while the volume of garbage entering every day is ± 125-130 m^3 / day. According to the manager of the Bulusan landfill, the Excavator with a capacity of 1.20 m^3 per hour is able to efficiently garbage 103 m^3, while for the Bulldozer operations with a capacity of 3.18 m^3 it is able to efficiently garbage up to 120 m^3 / hour. Calculation of the effectiveness of the machine as follows.

It's Known :

Excavator / hour heavy equipment operations = 103 m^3
Bulldozer / hour machine operation = 120 m^3
Effective working hours = 6 hours

The result of the assumption:

Operations/excavator days = Operational per hour × Effective working hours
= 103 m^3 × 6 hours = 618 m^3 / day
Operational / bulldozer day = Operational per hour × effective working hours
= 120 m^3 × 6 hours = 720 m^3 / day
Operational / year excavators = Operations per day × (1-day work time)
= 618 × (365 days - 96 days)
= 166242 m^3 / year
Operational / bulldozer year = Operations per day × (1-day work time)
= 720 × (365 days - 96 days)
= 193680 m^3 / year
The work volume of excavators and bulldozers = ((618 m^3/day + 720 m^3/day)) / (6 hours)
= 223 m^3/ day, or
= 59987 m^3/year

It is known that the monthly Bulusan landfill garbage data = 3987 m^3/month, or 47845 m^3/year. So the optimization coefficient of garbage volume is = 59,987 / 47,845 = 1.25.

The calculation of the capacity of machinery aims to determine the projection of the capacity of the Bulusan landfill with garbage efficiency through the operation of heavy equipment. The volume of garbage per year is reduced by the volume of excavators and bulldozers operations which is equal to 59987 m^3 or 1.25 of efficiency.

To further optimize the efficiency of reducing the volume of garbage in the Bulusan Landfill, additional machinery is needed, namely: Excavators and Bulldozers. Calculation for adding machine units:
The number of excavator units needed;
n = (largest production equipment) / (Production of tools)
= (223 m³ / day) / (103 m³ / hour)
= 2.16 (2 units)
The number of bulldozer units needed;
N = (largest production equipment) / (Production of tools)
= (223 m³ / day) / (120 m³ / hour)
= 1.89 (2 units)

3.6. Projection of Bulusan Landfill Capacity

From the projection of the capacity of the Bulusan TPA for 2018 the capacity has been overloaded with a height of 16.03 m and has been unable to accommodate 9,810 m^3 of garbage. Whereas in the next 15 year projections from 2017 to 2031, the Bulusan landfill is predicted to have overloaded 326.164 m^3 with embankment height of 49.28 m from the planned embankment height of 15 m, so that it has exceeded the planned capacity of 142,710 m^3 (overload). From the results of measurements in 2017 the height of landfill in the field reaches ± 13-14 meters, and in 2018 the heap height reaches ± 16-17 meters and according to the projection results, the embankment height has reached 16.03 meters. So the planned capacity has been exceeded, and it can be said that the capacity of the Bulusan landfill is dead and a replacement for the landfill site is needed. The projection of the capacity of the Bulusan landfill is presented in Table 6.

Table 6. Projections for Bulusan Landfill Capacity with Garbage Efficiency through Machinery Operations

year	Total populations	garbage (m^3)	Optimization of garbage Compaction (m^3)	Cumulative garbage Volume (m^3)	capacity (m^3)	Heap height (m)	Rest of capacity (m^3)
2006	924.171	27.621	22.030	22.030	8.812	0,93	133.898
2007	930.580	32.792	26.155	48.185	19.274	2,03	123.436
2008	927.656	30.433	24.273	72.458	28.983	3,05	113.727
2009	930.902	33.052	26.362	98.820	39.528	4,15	103.182
2010	930.399	32.646	26.038	124.858	49.943	5,25	92.767
2011	926.092	29.171	23.267	148.125	59.250	6,23	83.460
2012	927.879	30.613	24.417	172.541	69.017	7,25	73.693
2013	929.672	30.880	24.630	197.171	78.868	8,29	63.842
2014	943.686	45.172	36.029	233.200	93.280	9,80	49.430
2015	948.231	44.084	35.161	268.361	107.344	11,28	35.366
2016	942.428	44.524	35.512	303.873	121.549	12,78	21.161
2017	944.290	47.149	37.605	341.478	136.591	14,36	6.119
2018	*946.155*	*49.928*	*39.822*	*381.300*	*152.520*	*16,03*	*(9.810)*
2019	948.024	52.871	42.169	423.470	169.388	17,80	(26.678)
2020	949.897	55.987	44.655	468.125	187.250	19,68	(44.540)
2021	951.774	59.288	47.288	515.413	206.165	21,67	(63.455)
2022	953.654	62.783	50.075	565.488	226.195	23,77	(83.485)
2023	955.538	66.483	53.027	618.514	247.406	26,00	(104.696)
2024	957.425	70.402	56.152	674.667	269.867	28,37	(127.157)
2025	959.317	74.552	59.463	734.129	293.652	30,87	(150.942)
2026	961.212	78.947	62.968	797.097	318.839	33,51	(176.129)
2027	963.111	83.601	66.679	863.776	345.511	36,32	(202.801)
2028	965.013	88.529	70.610	934.386	373.755	39,28	(231.045)
2029	966.920	93.747	74.772	1.009.158	403.663	42,43	(260.953)
2030	968.830	99.273	79.180	1.088.338	435.335	45,76	(292.625)
2031	970.744	105.125	83.847	1.172.185	468.874	49,28	(326.164)

3.7. The Bulusan Landfill Needs Analysis

To find out the land needs for replacing the Bulusan landfill we calculate for 15 years planning capacity. It has been know that the population served for the next 15 years in 2031 is 970,744 people, The rate of landfill (R) is 0.70 kg/person/day, Operating Period is 15 years, Assumption of garbage density (D) is 250 kg/m^3, percentage of volume reduction after solidification (P) is 60%, High solid garbage and overburden which planned is 16 m. So the calculations is

$R = 0.70 \times 365 = 256$
$P = 60\%$
$D = 250\ kg\ /\ m^3$
$V = 1.25\ x\ (256/250)\ x\ (1\ -\ ((60\%)\ /\ 100)$
$= 0.51 m^2\ /\ person\ /\ year$
Land area (A):
$= ((0.51\ x\ 970{,}744))\ /\ 16\ =\ 31{,}003\ m^2\ /\ year$
$= (31{,}003 m^2\ /\ year)\ /10{,}000\ =\ 3.10\ ha$
New landfill needs:
$= 3.10\ x\ 15\ =\ 46.50\ ha$
$= 46.50\ x\ 10{,}000\ =\ 465{,}047\ m^2$
So the demand for Bulusan landfill is planned at 46.50 ha or 465,047 m².

Based on the results of [6], the determination of the location of candidates for the replacement of the Bulusan landfill based on the Geographic Information System is located at 114 ° 21'45.0 "- 114 ° 22'13.2" BT and 8 ° 06'14.5 "-8 ° 06 ' 36.3 "LS in Ketapang Village, Kalipuro District, Banyuwangi Regency, with area is 0.4641 Km² or 46.41 Ha. the amount of land needed from the selection results of the Geographic Information System is in line with the projected landfill needs for the next 15 years.

4. CONCLUSION

From the projection it has been declared that the Bulusan landfill capacity in 2018 is overloaded with the height of the embankment is 16.03 m, and has been unable to accommodate trash of 9.810 m. in the next 15 year projections from 2017 to 2031, the Bulusan landfill will be overloaded 326.164 m³ of garbage with embankment height is 49.28 m. for the next 15 years the area needed is 46.50 ha or 465,047 m². A financial and technical feasibility study is needed for potential replacements for the Bulusan Landfill so that it can be immediately realized as a pilot project as a replacement for the Bulusan landfill.

5. ACKNOWLEDGEMENT

Thanks to Politeknik Negeri Banyuwangi who funded the Beginner's Lecturers' Research through DIPA PNBP funding in 2018.

6. REFERENCES

[1] E. Damanhuri and T. Padmi, *Diktat Kuliah Pengelolaan sampah*. 2010.
[2] M. Audina, S. Anwar, and Y. Antomi, "Prediksi dan Analisis Tempat Pembuangan Akhir (TPA) Sampah di Kota Padang Prediction and Analysis of Final Waste Dumps in Padang City," in *Seminar nasional Penginderaan Jauh*, 2018, pp. 1–9.
[3] H. Jimmyanto, I. Zahri, M. H. Dahlan, and S. N. R. Putri, "EVALUASI SISTEM PENGELOLAAN SAMPAH PADAT DOMESTIK DI KOTA PALEMBANG TAHUN 2017," *Demogrphy J. Sriwij.*, vol. 6, no. 1, pp. 1–7, 2017.
[4] R. Yanto, "Implementasi Data Mining Estimasi Ketersediaan Lahan Pembuangan Sampah menggunakan Algoritma Regresi Linear Robi," *J. RESTI*, vol. 2, no. 1, pp. 361–366, 2018.
[5] Mesran, D. I. Zalukhu, S. Handayani, and D. U. Sutiksno, "Penerapan WASPAS dan MOORA Dalam Menentukan Lokasi Tempat Pembuangan Sampah Akhir," in *Seminar Nasional Sains & Teknologi Informasi (SENSASI)*, 2018, pp. 347–353.
[6] Z. Erwanto and A. Holik, "Determination Study of Landfill Location As A Potential Replacement For Bulusan Landfill Using Geographic Information System," in *International Conference on Applied Science and Technology (iCAST)*, 2018.

LOGIC
Journal of Engineering Design and Technology
Vol. 19 No.3 November 2019; p. 115 - 119

p-ISSN : 1412-114X
e-ISSN : 2580-5649
http://ojs.pnb.ac.id/index.php/LOGIC

ENERGY ANALYSIS PRODUCED IN MIXTURE OF LIQUID (PERTALITE) AND GAS (LPG) IN CONVENTIONAL MACHINE 4 CYLINDER

Adi Pratama Putra[1)], Ikhwanul Qiram[2)]

[1,2] Mechanical Lecturers in Mechanical Engineering Department, Universitas PGRI Banyuwangi
Ikan Tongkol street No. 22 Kertosari, Banyuwangi, East Java, Indonesia

Correponding email [1,2] :
tama.adie@yahoo.com
ikhwanulqiram@gmail.com

Abstract. *Increased mobility of transportation plays a major role in the economic growth of a region. Despite the rapid growth of the automotive industry, there are still quite a lot of people who use old-type vehicles to support their mobility. Conventional 4-cylinder engine is one type of engine that is widely used in public transportation modes. The purpose of this study was to obtain an analysis of the energy produced in a mixture of liquid fuel (pertalite) and gas (LPG) in a conventional engine 4-cylinder. The research method used was an experiment, carried out on a conventional engine 4-cylinder. A dynamometer is used to determine the power and torque produced. As for testing the rate of fuel consumption using a measuring burette, then the fuel consumption is calculated. The research data are arranged in tables and graphs to obtain the analysis of the energy produced at each rotation speed variation (Rpm). The results showed there were differences in power, torque and fuel consumption produced by a mixture of the two types of fuel used. For maximum power generated at a standard injector variation that uses Pertamax plus fuel of 11.61 kW and a maximum torque of 12.98 Nm. While the lowest power is produced by Pertamax using a racing injector of 2.26 kW and the lowest torque of 8.67 Nm. The lowest fuel consumption is obtained from the use of a standard fuel injector Pertamax plus of 0.12 kg / kW while the highest fuel consumption produced by Pertamax Plus uses a standard injector of 1.28 kg / kW.*

Keywords : Energy, mixed, liquid fuel, gas

1. INTRODUCTION

The number of studies on natural gas (LPG) applied to vehicles is a step and effort to find alternative fuels, in it's development the majority of studies only incorporate natural gas into the combustion chamber using conventional types of vehicles or injection vehicles.

Liquid fuel is a combination of hydrocarbon compounds obtained from nature and artificially. Liquid fuels are generally derived from petroleum, in the future, the possibility of liquid fuels derived from oil shale, tar sands, coal and biomass will increase. Petroleum is a natural mixture of liquid hydrocarbons with little sulfur, nitrogen, oxygen, very little metal, and minerals [1].

Gas fuel is a compressed natural gas. In general, more than 80% of the natural gas component used as CNG is methane gas, 10% -15% ethane gas, and the rest is carbon dioxide gas, and other gases, the composition of BBG used in Jakarta 93% consists of methane gas , 3.2% ethane gas, and the remaining 3.8% are nitrogen, propane, and carbon dioxide, the composition of the natural gas varies from one source to another [2].

Study comparative of gasoline fuel energy with gas fuel in motor vehicles, the results obtained from the use of gas fuel energy is more efficient up to 10% compared to Gasoline fuel, with the overall power (kW) on gas-fueled engines 2% smaller to 5% compared to gasoline fuel, this value shows the performance of the engine with gas fuel is not as good as the Gasoline engine [3]. The difference of octane rate will give significant impact to emision characteristic when using different rate of octane showing differen percentage [4]. The use of LPG fuels as an alternative to conventional engine is very likely to be more efficient than fossil fuels [5].

From the description above it can be concluded, most research on the change of liquid fuel to gas fuel, not a mixture of the two fuels, so researchers here will examine the Effect of Mixing Liquid Fuel (Pertalite) and Gas Fuel (Lpg) Against Fuel Consumption in Conventional 4-cylinder engine, is it able to be more economical by mixing the two fuels into the combustion chamber.

2. METHODS

Mindset of research as follow:

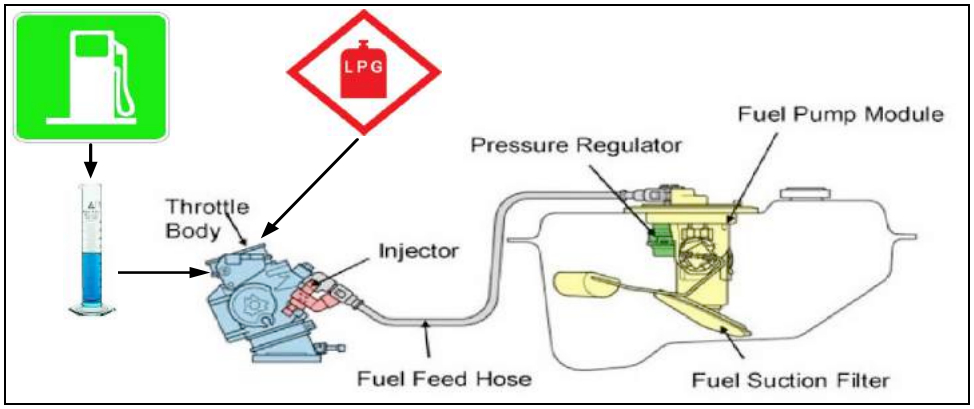

Figure 1. Mindset

Research variables

1) Independent variable:
   a. 4 variations of Rpm: 1000, 1500, 2000 and 2500 Rpm
   b. 4 variations of fuel discharge: 0.9; 1.4; 1.8; and 2.2 ml/sec
   c. Fuel : pertalite and liquified Petroleum gas (LPG)

2) Dependent variable: engine power

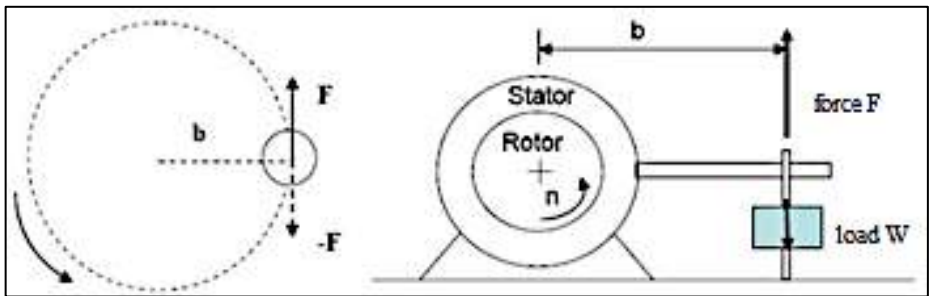

Figure 2. research measurement techniques

The dynamometer is used to measure the power, torque generated by the engine after it is given variations in the treatment of fuel mixture types.

3. RESULTS AND DISCUSSION

3.1 Figur And Table

The data obtained from the research through observation and experiment still needs to be processed. The processed data results in the average value and then it is tabulated in table.

Table 1 Data collection table for liquid fuel consumption (pertalit) without the addition of LPG

Type of Fuel	(RPM)	Used Fuel (ml)	Time (sec)	Consumption / time	Average Time (ml/sec)
Pertalite	1000	10	44,58	0,22	0,22
		10	46,5	0,21	
		10	45,02	0,22	
	1500	10	28,2	0,35	0,36
		10	27,2	0,36	
		10	27,6	0,36	
	2000	10	24,7	0,4	0,42
		10	23,9	0,41	
		10	23,2	0,43	
	2500	10	18,9	0,52	0,56
		10	17,7	0,56	
		10	17,2	0,58	

Table 2 Table of results of taking data on liquid fuel consumption (pertalit) with the addition of LPG

Type of Fuel	(RPM)	Used Fuel (ml)	Time (sec) with LPG	Anemometer m/s
Perttalite & LPG	1000	10	50	0,9
	1000	10	49,9	0,9
	1000	10	49,1	0,9
	1500	10	38,8	1,4
	1500	10	38,3	1,4
	1500	10	38,6	1,4
	2000	10	34,1	1,8
	2000	10	34,9	1,8
	2000	10	34,7	1,8
	2500	10	27,5	2,2
	2500	10	26,7	2,2
	2500	10	27,1	2,2

Table 3 Table of calculation of average results and percentages

RPM	Average Time (Sec) Pertalite	Average Pertalite & LPG	Difference Time (Sec)	Percentage
1000	45,37	49,67	4,3	1,95
1500	27,67	38,57	10,9	3,02
2000	23,93	34,57	10,63	2,54
2500	17,93	27,1	9,17	1,64
Average Difference			8,75	2,29

The Graphic of the Research Result

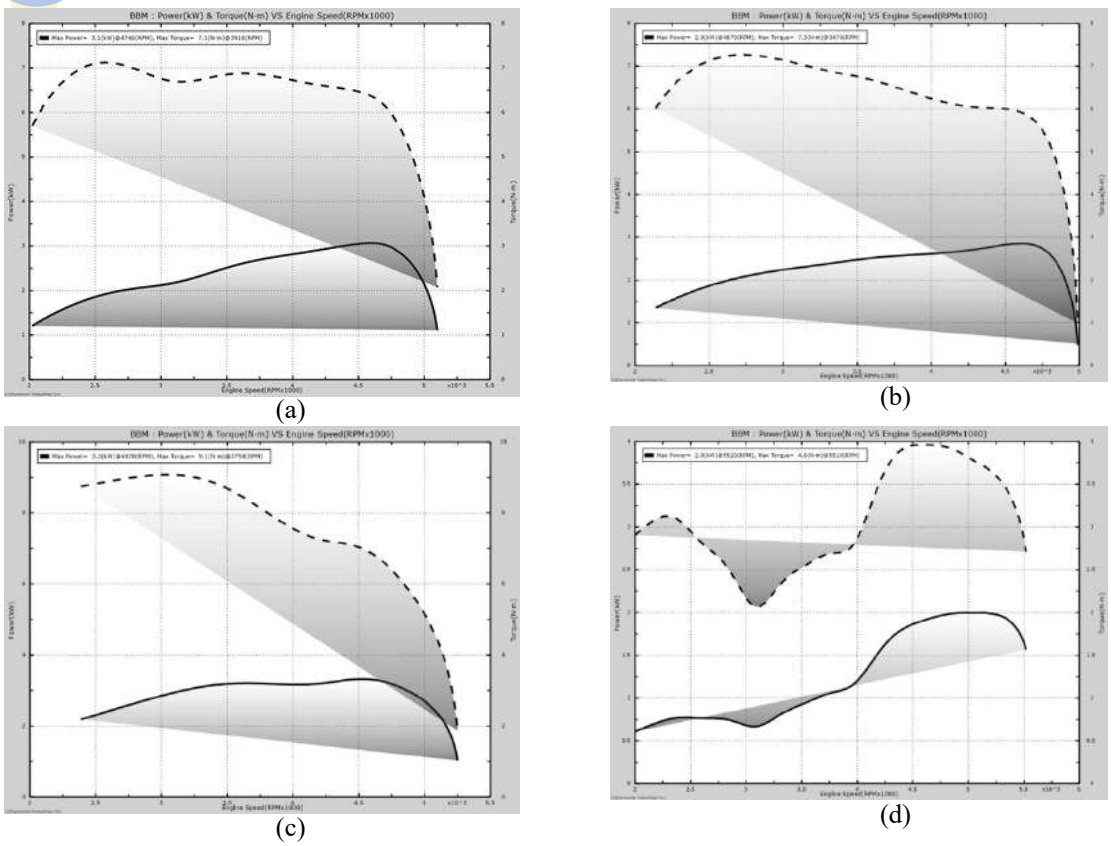

(a) (b) (c) (d)

Figure 2. Histogram power and torque with pertalite

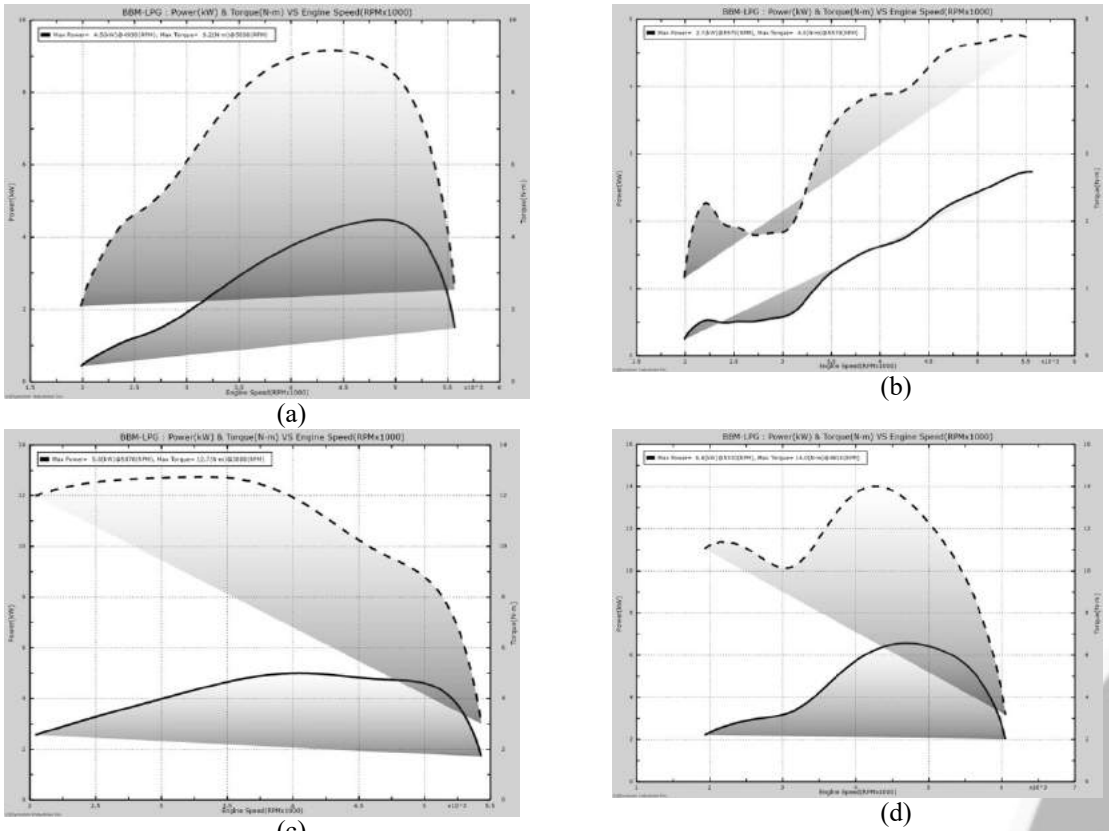

(a) (b) (c) (d)

Figure 3. Histogram power and torque with pertalite and LPG

Based on figures (2) and (3), the test results show that there is a difference between the torque using pertalite fuel oil and LPG gas fuel. As rpm increases torque using pertalite decreases. Maximum torque at pertalite is 4470

rpm at 3.1 Kw and minimum torque is at 3910 rpm at 7.1 Nm. While the maximum torque at LPG is at 4930 rpm at 4.5 Kw, and the minimum torque at 5090 rpm at 9.2 Nm. This means that the difference in torque between pertalite fuel and LPG gas is significant. In other words there is a significant difference in motor torque by using pertalite fuel oil and LPG gas fuel.

Research on the conversion of fuel oil to natural gas produces lower torque and power in the use of LPG gas fuel compared to using pertalit fuel, this occurs because in the use of pertalite fuel with octane (RON) 90 the maximum yield of combustion pressure because it is supported by compression pressure and also when proper ignition so that the resulting torque is also maximum. Whereas in the use of LPG gas with octane (RON) 112 the combustion pressure is not maximal because it is not supported by high compression pressure and also during proper ignition so that the resulting torque is also not maximal. Based on data obtained from the difference in motor torque using pertalite fuel oil and LPG gas fuel, variations in engine speed and the use of fuels with different octane values will affect the value of torque produced. This can be proven by the results of the study in figures (2) and (3), when the rpm is increased the torque using pertalite decreases.

Power is the amount of effort done by the motor in a period of time or the results of the effort divided by a certain period of time. The amount of power produced is very influential on variations in engine speed and the effect of the fuel which has different octane values. As rpm increases, power using pertalite tends to increase. From the test results show that motor torque using pertalite fuel is higher than motor torque using LPG gas fuel and motor power using pertalite fuel which is higher than motor power using LPG gas fuel.

There is a significant difference in motor power using pertalite fuel oil and LPG gas fuel. So that in motor research using pertalite fuel oil produces higher torque and power compared to using LPG gas fuel. The causes of torque and motor power generated are small in the use of LPG gas fuel, namely, a) The speed of energy per unit volume owned by LPG gas is lower than gasoline fuel, especially pertalite, so the combustion energy decreases, b) LPG has more carbon chains shorter than pertalite, c) LPG has a short hydrocarbon (CH) chain than pertalite, so that the total energy and peak combustion pressure resulting from the LPG combustion process is not as much as that produced in the pertalite combustion process, d) LPG gas pressure entering the chamber the fuel is constant, but the inlet air pressure changes, so that the torque and power of the LPG usage are lower than the pertalite, and e) The better the converter kit is used, the better performance.

4. CONCLUSION

The conclusions that the author can give from the effect of the comparison of the use of LPG gas fuel and pertalite fuel on the performance of this 4 stroke gasoline fuel motor are as follows :

1. There is a significant difference in motor torque by using pertalite fuel oil and LPG gas fuel.
2. There is a significant difference in motor power using pertalite fuel oil and LPG gas fuel.
3. Maximum torque at pertalite is 4470 rpm at 3.1 Kw and minimum torque is at 3910 rpm at 7.1 Nm. While the maximum torque at LPG is at 4930 rpm at 4.5 Kw, and the minimum torque at 5090 rpm at 9.2 Nm

5. ACKNOWLEDGEMENT

We would like to say thank you very much to:

1. Rector of PGRI University of Banyuwangi and and all his staff.
2. Ministry of Research, Technology and Higher Education; Beginner Lecturer Research Program in Fiscal Year of 2019.

6. REFERENCES

[1] Wiratmaja. 2010. *Pengujian Karakteristik Fisika Biogasoline Sebagai Bahan Bakar Alternatif Pengganti Bensin Murni*, Jurnal Ilmiah Teknik Mesin Vol. 4 No.2. Oktober 2010.

[2] Tulus. 2002. *Tinjauan Pengembangan Bahan Bakar Gas Sebagai Bahan Bakar Alternatif*. Journal Digitalized by USU digital library.

[3] Ozkar, Ambo, Septian. 2015. *Studi Perbandingan energi bahan bakar gasoline dengan bahan bakar gas pada kendaraan bermotor*. Jurnal desiminasi teknologi, Volume 3, No. 2, Juli 2015.

[4] I Putu Sastra Negara, I Made Arsawan. 2014. Optimalisasi Penggunaan Bahan Bakar Kendaraan Bermotor Untuk Menghasilkan Gas Buang Yang Ramah Lingkungan. Jurnal logic. Vol. 14. No. 1. Maret 2014

[5] Djoko, Rizal. 2015. *Komparasi Penggunaan Bahan Bakar Premium Dengan Bahan Bakar LPG System Manifold Injeksi Terhadap Kadar Emisi Gas Buang Sepeda Motor 4 Langkah*. Jurnal Institute Teknologi Adhi Tama Surabaya.

LOGIC
Journal of Engineering Design and Technology
Vol. 19 No.3 November 2019; p. 120 - 130

p-ISSN : 1412-114X
e-ISSN : 2580-5649
http://ojs.pnb.ac.id/index.php/LOGIC

MOBILE APPLICATION SEARCHING OF THE SHORTEST ROUTE ON DELIVERY ORDER OF CV. ALFA FRESH WITH BRUTE FORCE ALGORITHM

Indri Ariyanti[1)], M. Aris Ganiardi[2)], Ulsa Oktari[3)]

1,2,3) Politeknik Negeri Sriwijaya, Jl Srijaya Negara Bukit Besar Palembang 30139, Indonesia.

Correponding email [1)] : indri@polsri.ac.id

Abstract. Traveling Salesman Problem is a problem solving used in finding the shortest route to visit all nodes at once and then return to the initial node. Troubleshooting of the Traveling Salesman Problem using the Brute Force algorithm. The object of this research is the courier at CV. Alfa Fresh. The Brute Force algorithm provides a solution for Traveling Salesman Problems to select and determine the shortest routes to deliver orders from the office to the destination. Methode The Brute Force algorithm is methode an algorithm that is used to match patterns with all routes to be traversed to find the shortest route pattern. Result in reseach is the Brute Force algorithm works by enumerating all possible candidates. With this application can facilitate the courier in determining the closest route from the position of the courier. This application can also be a note for the courier to see what order he did. The brute force algorithm can give the shortest route from the courier position well, but the calculation process is a little slower because the algorithm calculates all possible distances.

Keywords : Traveling Salesman Problem, *Brute Force* Algorithm, Shortest Route.

1. INTRODUCTION

CV. Alfa Fresh is an Indonesian company that provides purchasing services for online kitchen needs such as selling fruits, vegetables, meat and other kitchen spices. CV. Alfa Fresh was founded in 2017 in the city of Palembang. This company provides Web and Mobile based applications for marketing. CV. Alfa Fresh itself has many employees with various kinds of parts, one of which is courier. Courier in CV. Alfa Fresh is in charge of delivering orders as well as to other companies, couriers who help buyers to deliver their orders who ordered online.

Couriers visit the place of the customer, where the place or destination of the courier not only one place but several places each day according to the order received. And only need to be delivered once for each customer. If there are 5 places / destinations to be visited by the courier, then there are several routes that may be passed. This causes the courier to be able to arrange the order of his visit in order to get the most effective distance possible. The problem that often occurs is that couriers sometimes forge distances that are too far and too swirling to visit one place to another, this causes couriers to be less efficient in visiting the order in which they want to go.

Resolving the problem of traveling salesman problems can be applied to visiting a number of places. To solve this problem there are various methods that can be used, one of them is by using the Brute Force algorithm. The Brute Force algorithm is an algorithm that is used to match patterns with all routes that will be passed to find

The optimal route pattern. Brute Force is a very common problem solving technique and can be used to solve problems by finding the shortest route. Brute Force works by enumerating all possible candidates, giving the best solution. The shortest route is a problem to find a path between two or more vertices in a graph weighted with the minimum number of graph side weights crossed. In weighted graphs there are optimizations that can be expressed in distances between cities, message delivery times, costs and so on. In this case the weight must be

positive, although in other cases it can be negative. The shortest path with the initial vertex s and vertex t destination is defined as the shortest path from s and t with minimum weight and in the form of a simple path [1]. What is done in TSP is forming a travel route. The operator that can be used for Travelling Salesman Problem (TSP) problems is the search for sequences of all locations to select locations that have not been selected one by one so that a complete route of visit is generated from the initial location then visits all other locations exactly once and finally returns to the original location [2].

TSP is divided into 2 types, namely: (1) Asymmetrical TSP, this type of Asimetirs TSP, the cost from city 1 to city 2 is not the same as the cost from city 2 to city 1, with n cities, the size of the search space is a possible path; (2) symmetrical TSP, the type of Symmetrical TSP, the cost from city 1 to city 2 is the same as the cost from city 2 to city 1. If with n cities, the number of possible routes is a possible path.

The Brute force method is a direct approach to solving a problem, which is based on problem statements and defines the concepts involved directly. Troubleshooting using the Brute force Method is very simple, direct and clear. Characteristics of the Brute force method: (1) The number of steps needed is large, (2) Used as a basis for finding a more efficient or creative solution, (3) Almost all problems can be solved by this method, (4) Used as a basis in comparing the quality of an algorithm [3].

Exhaustive search is a brute force solution search technique for problems that involve finding elements with special properties. Usually between combinatory objects such as permutations, combinations, or subsets is part of a set [4]. The use of Brute force on TSP problems can be illustrated as follows: Given many (n) destinations in a city and the distance between each city is known to each other. Find the shortest tour through every other city only once and return to the city from departure. This TSP problem is nothing but finding a Hamilton circuit with a minimum weight. *Exhaustive search* technique steps*:* (1) Make a list (Enumeration) of every possible solution in a systematic way, (2) Evaluate each possible solution one by one, especially the mirror solution, can be issued. Then save the best solution to date (3) After the search ends, announce the best solution, (4) The resources needed in finding solutions using *Exhaustive Search* are very large, although the exhaustive technique theoretically produces a solution.

In order for the mobile application to be utilized by the courier at the company, mobile applications that can replace orders based on the customer's address is needed, then determine the order of the shortest route to be traversed from the data that has been collected. For this reason, research was carried out on Mobile Application Searching of the Shortest Route on Deliver Order of CV. Alfa Fresh with the Brute Force Algorithm. The Mobile Application is expected to help the courier officer on the CV. Alfa Fresh to determine the shortest route to visit customers so that it can shorten the distance traveled and save time.

This study focuses on the analysis, design, and development of EzDelivery which implements the Held-Karp and Fixed-Radius Near Neighbors algorithm (Castillo, Reynaldo E.Agustin, et al : 2019). The fixed-radius near neighbors algorithm is used to find the closest company because of its effectiveness in achieving mobile application functionality.

2. METHODS

2.1 Stage of Research Problems

This stage is the process of formulating problems and limiting the problems to be studied. This is needed in order to be able to better direct the researcher in making the application so that what is done is not out of the predetermined limits.

2.2 Data Collection

In this data collection stage the author refers to opinions [5], where the opinions explain the stage of data collection which is divided into two types, namely:

1. Primary Data

Primary data is data that was first recorded and collected in the study. Primary data where the author conducts a survey directly to the party concerned, namely the party that has the authority to collect the data. The author conducted interviews and observations with employees of CV. Alfa Fresh Palembang. The interview produced an obstacle faced by the CV. Alfa Fresh Palembang where the courier as the delivery order to the customer is still constrained in determining the most effective route to deliver orders to customers, so that the time of shipping orders is still less effective.

2. Secondary Data

Secondary data is data collected from existing sources. Here, here the author collects data indirectly, namely by searching for information through research journals, books, and other document sources, as a reference for the construction of mobile applications that will be made.

2.3 Research Design

In doing this final project, the system design used includes usecase diagrams, activity diagrams, class diagrams, and sequence diagrams.

2.4 Completion of the Brute Force Algorithm With Exhaustive Search Technique On Traveling Salesman Problem

An example of a case study of the application of a brute force algorithm with the Exhaustive Search technique on the Traveling Salesman Problem itself is as follows, with a starting position at CV.Alfa Fresh then the first point to Jalan Putri Rambut Selako no.4 Ilir barat 1, second point Jalan Joko No. 10 Small hill, and third point Jalan Bali Blok C3 Complex Pusri Borang Sako then return to CV. Alfa Fresh.

Table 1 List Order

Position	Latitude	Longitude
Cv. Alfa Fresh (A)	-2.9439079	104.7327026
Jalan Putri Rambut Selako No.4 Ilir barat 1 (B)	-2.9934064	104.7300526
Jalan Joko No 10 Bukit Kecil (C)	-2.9930219	104.7480037
Jalan Bali Blok C3 Komplek Pusri Borang sako (D)	-2.9252864	104.7794028

First, look for the distance between the starting positions to the destination with the euclidean distance calculation formula, namely:

$$d_{ij} = \sqrt{[(x_i - x_j)^2 + (y_i - y_j)^2]} \quad (1)$$

Information
x_i = Coordinate x for initial point i (latitude)
y_i = Coordinate y for destination point j (longitude)
d_{ij} = Distance between two points i and j

Looking for the distance between the initial start, namely CV. Alfa Fresh to the destination Jalan Putri Rambut Selako No. 4 Ilir barat 1 (A-B) with the following formula :

$$d_{ij} = \sqrt{[(x_i - x_j)^2 + (y_i - y_j)^2]}$$
$$= \sqrt{((-2.9439079) - (-2.9934064)^2 + ((104.7327026) - (104.7300526)^2)}$$
$$= \sqrt{(0.0494985)^2 + (0.00265)^2}$$
$$= \sqrt{(0.002450101502 + 0.0000070225}$$
$$= \sqrt{0.002457124002}$$
$$= 0.049569385733 \text{ X } \frac{111.322}{1000}$$
$$= 0.0005518163159$$

Looking for the distance between the initial start, namely CV. Alfa Fresh to the destination of Jala Joko No. 10 Small hill (A-C) with the following formula:

$$d_{ij} = \sqrt{[(x_i - x_j)^2 + (y_i - y_j)^2]}$$
$$= \sqrt{((-2.9439079) - (-2.9930319)^2 + ((104.7327026) - (104.7480037)^2)}$$
$$= \sqrt{(0.049124)^2 + (0.0153011)^2}$$

$= \sqrt{(0.002413167376 + 0.0002341236612}$
$= \sqrt{0.0026472910372}$
$= 0.0514518322045 \text{ X } \frac{111.322}{1000}$
$= 0.005727720865$

Looking for the distance between the initial start, namely CV. Alfa Fresh to the destination of Jalan Bali Blok C3 Komplek Pusri Borang sako (A-D) with the following formula:

$$d_{ij} = \sqrt{[(x_i - x_j)^2 + (y_i - y_j)^2]}$$
$$= \sqrt{((-2.9439079) - (-2.9252864)^2 + ((104.7327026) - (104.7794028)^2)}$$
$$= \sqrt{(-0.0186215)^2 + (-0.0467002)^2}$$
$$= \sqrt{(0.0003467026225 + 0.00218090868004}$$
$$= \sqrt{0.00252766894229}$$
$$= 0.05027592805996 \text{ X } \frac{111.322}{1000}$$
$$= 0.00559681686349$$

Looking for the distance between the initial start, namely Jalan Putri Rambut Selako No. 4 Ilir barat 1 to the destination of Jalan Joko No.10 Bukit Kecil (B-C) with the following formula:

$$d_{ij} = \sqrt{[(x_i - x_j)^2 + (y_i - y_j)^2]}$$
$$= \sqrt{((-2.9934064) - (-2.99330319)^2 + ((104.7300526) - (104.7480037)^2)}$$
$$= \sqrt{(-0.0003745)^2 + (-0.0179511)^2}$$
$$= \sqrt{(0.00000014025025 + 0.00032224199121}$$
$$= \sqrt{0.00032238224146}$$
$$= 0.01795500602785 \text{ X } \frac{111.322}{1000}$$
$$= 0.00199878718103$$

Looking for the distance between the initial start, namely Jalan Putri Rambut Selako No. 4 Ilir barat 1 to the destination of Jalan Bali Blok C3 Komplek Pusri Borang sako (B-D) with the following formula:

$$d_{ij} = \sqrt{[(x_i - x_j)^2 + (y_i - y_j)^2]}$$
$$= \sqrt{((-2.9934064) - (-2.9252864)^2 + ((104.7300526) - (104.7794028)^2)}$$
$$= \sqrt{(-0.06812)^2 + (-0.00493502)^2}$$
$$= \sqrt{(0.0046403344 + 0.00243544224004}$$
$$= \sqrt{0.00707577664004}$$
$$= 0.08411763572545 \text{ X } \frac{111.322}{1000}$$
$$= 0.00936414344423$$

Finding the distance between the initial start, namely Jalan Joko No. 10 Small hill to the destination of Jalan Bali Blok C3 Komplek Pusri Borang sako (C-D) with the following formula :

$$d_{ij} = \sqrt{[(x_i - x_j)^2 + (y_i - y_j)^2]}$$
$$= \sqrt{((-2.9930319) - (-2.9252864)^2 + ((104.7480037) - (104.7794028)^2)}$$
$$= \sqrt{(-0.064745)^2 + (-0.0313991)^2}$$
$$= \sqrt{(0.004322405025 + 0.000985903480}$$
$$= \sqrt{0.005308308505}$$
$$= 0.07285813959332 \text{ X } \frac{111.322}{1000}$$
$$= 0.00811071381581$$

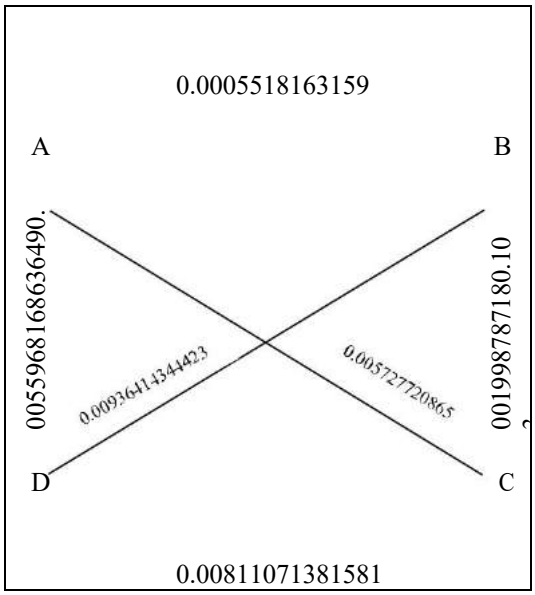

Figure 1 Illustration results of calculation of order distance

After searching for distances, we can get all the weights of all distances and we must calculate each weight, and choose the Hamilton circuit with the smallest weight.

R1 = (A,B,C,D,A) = 0.0005518163159 + 0.001998787 18103 + 0.00811071381581 + 0.00559681686349
= 0.01625813417623

R2 = (A,B,D,C,A) = 0.0005518163159 + 0.009364143 44423 + 0.00811071381581 + 0.005727720865
= 0.02375439444094

R3 = (A,C,B,D,A) = 0.005727720865 + 0.0019987871 8103 + 0.00936414344423 + 0.00559681686349
= 0.02268746835375

R4 = (A,C,D,B,A) = 0.005727720865 + 0.0081107138 1581 + 0.00936414344423 + 0.0005518163159
= 0.02375439444094

R5 = (A,D,B,C,A) = 0.00559681686349 + 0.00936414 344423 + 0.00199878718103 + 0.005727720865
= 0.02268746835375

R6 = (A,D,C,B,A) = 0.00559681686349 + 0.00811071 381581 + 0.00199878718103 + 0.0005518163159
= 0.01625813417623

So the calculation of the *exhaustive search* technique above can be done to repair the number of route searches, namely by knowing that half of the travel routes are the result of reflection of the other half route, that is by changing the direction of the route, the route is:
R1 dan R6 = 0.01625813417623
R2 dan R4 = 0.02375439444094
R3 dan R5 = 0.02268746835375

Then the route chosen based on the total distance of the smallest or closest is R1 and R6

2.5 System Development Method

If in making the application the author uses the *Brute Force* algorithm, then in developing the system the author uses the Waterfall system development method. The *waterfall* method is done in stages one by one starting from the top stage to the bottom stage. The stages involved include the analysis, design, coding, testing, and *support* phases. The *waterfall* development method was chosen because the application of steps in the *waterfall* was in accordance with the method of development carried out by the author.

a. Analysis of software requirements

The stage for analyzing the needs of external devices is the process of gathering system requirements such as Android Studio for editors coding applications; Sublime Text is useful to encode the web, MySql to store databases, PHP to encode php programs.

b. Design
The design stage is a needs analysis of system design software in use case diagrams, activity diagrams, class diagrams, and sequence diagrams.

c. Program code creation
The stage of making the program code is the process of doing coding system (Encoding Software) on Android Studio and Sumbile Text by the Programmer in accordance with the analysis and design stages that have been made before.

d. Testing
The testing phase of the author uses the Black Box method, testing is done to find out whether the system is running well and not. In conducting testing the author makes a test plan as a reference in conducting testing.

e. Support or maintenance
This maintenance stage checks the application system if there is a mistake, the application will be corrected.

3. RESULTS AND DISCUSSION

3.1 System Requirements Analysis

a. Functional Requirements

Rosa and Shalahudin [6], Explain functional requirements is a need related to product functions, for example, information systems must be able to print reports, information systems must be able to display graphics, etc.

The functional requirements of the system to be built are as follows:

1. The website and application system can authorize and authenticate users such as admin and courier.
2. The website system created can input data, edit data, and delete data in the form of admin, customer, order, order, product, user, and courier data.
3. The application system can search for the nearest route.
4. The application system can see the order history that has been completed.

b. Non Functional Requirements

Non-functional needs are additional needs that do not have inputs, processes, and outputs. However, this non-functional requirement should be fulfilled because it will determine whether this system will be used by the user or not.

The related non-functional needs are two, namely:

1. Admin websites that will be built include:
   a. The website must be accessible with a browser.
   b. The website must be accessible to the user formulated.
   c. Has a friendly user interface
   d. The website system has a password, so only registered users can access the website.

2. Courier applications to be built include:
   a. The ease of use of software can be accessed anywhere and anytime through mobile-based applications.
   b. Safety factors related to the use of the API Key (Application Programming Interface).

3.2 System Planning

a. Usecase Diagram

According to Rosa and Shalahuddin [6], use case diagram is a model for information system behavior to be created. The use case describes an interaction between one or more actors with the information system that will be created. Roughly speaking, usecase is used to find out what functions are in an information system and who has the right to use those functions.

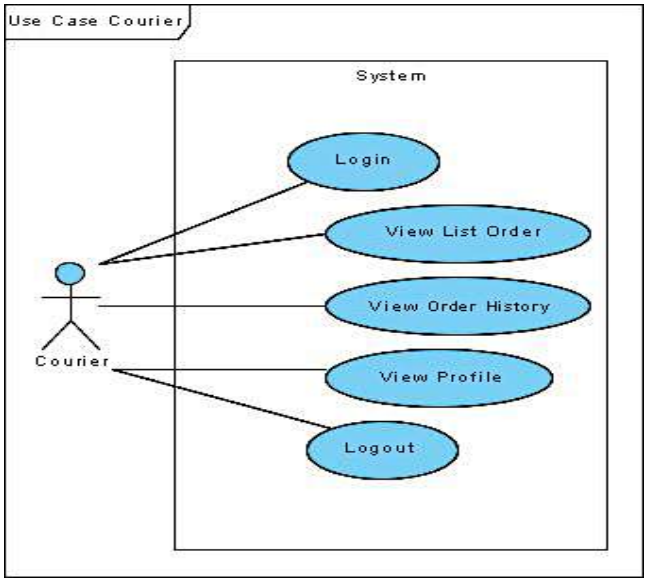

Figure 2 *Usecase* Courier Diagram

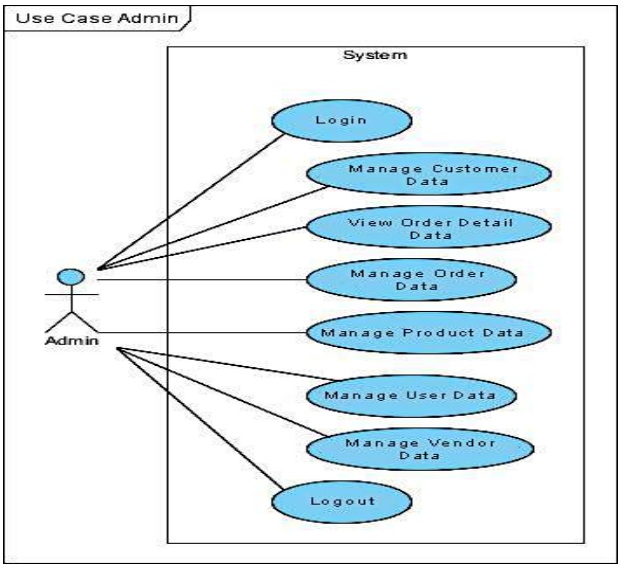

Figure 3 *Usecase* Admin Diagram

b. Class Diagram

Rosa and Shalahudin Class diagrams illustrate the system structure in terms of defining the classes that will be made to build the system [6]. Classes have what are called attributes and methods or operations. Attributes are variables owned by a class. Whereas, operations or methods are functions that are owned by a class.

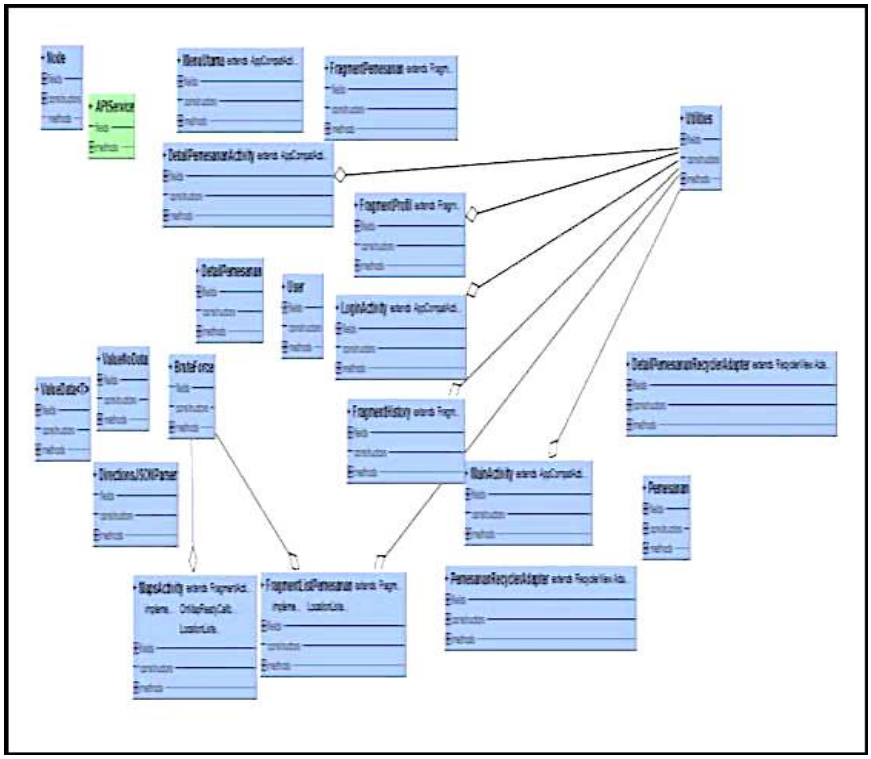

Figure 4 *Class* Application Diagram

3.3 System Implementation

The following is the interface of the system application:

Figure 5 Application Login Page

On this page the courier logs in first to access this application by filling in the username and password then press the login button. If successful the courier login can access on the next page.

Figure 6 Application List Order page

This main page functions to view the list of orders and by pressing the Access button Start the Route then the courier can find out the route of the order to be followed. In addition, this page contains 3 access panels in the form of Order Lists, order history, and profiles.

Figure 7 Start Page of the Application

It is a route map page for orders that are in the application. This page will help the courier get the shortest distance route to deliver orders and be accompanied by directions to directions such as those available in Google Maps.

Figure 8 Display the order history page of the application

This page is a page that will display order history if the courier has finished delivering customer orders.

Figure 9 Application Profile Display Page

This page is a page that will display the profile of the messenger and there is a logout button for the courier to exit the application.

4. CONCLUSION AND SUGGESTIONS

4.1 Conclusion

Based on the discussion described in the previous chapters, there are several conclusions is as follows:

a. With this application it can make easier for couriers to determine the closest route to the position of the courier.

b. This application can also be a note for the courier to see what order he did.
c. The brute force algorithm can give the shortest route from the courier position well, but the calculation process is a little slower because the algorithm calculates all possible distances.

4.2 Suggestions

As for suggestions that can be given by writer based on observations that have been done include:

a. It would be more useful if this application was added about kilometers that he had traveled to become a reminder to service the vehicle.
b. This mobile application will be better if it is equipped with feature receiver messages from the office.

5. REFERENCES

[1] Andayani Sri, Wulan Endah Perwitasari, (2014), Penentuan Rute Terpendek Pengambilan Sampah di Kota Merauke Menggunakan Algoritma Dijkstra, Seminar Nasional Teknologi Informasi dan Komunikasi Terapan 2014, ISBN: 979-26-0276-3, hal 165.
[2] Tri Dian Wiyanti, (2013), Algoritma Optimasi Untuk Menyelesaikan Travelling Salesman Problem, Jurnal Transformatika, vol 11, hal 2.
[3] Wilson, Yuliant, Izzatul, (2015), Analisis Penyelesaian Traveling Salesman Problem Dengan Metode *Brute Force* Menggunakan *Graphic Processing Unit*, e-Proceeding of Engineering, vol 2, hal 1875-1876.
[4] Munir, Rinaldi. Diklat Kuliah IF2251. *Strategi Algoritmik*
[5] Suryabrat Sumadi, (2015), Metodelogi Penelitihan, Jakarta, Rajawali Pers.
[6] A.S Rosa , dan M. Shalahuddin. (2014). *Rekayasa Perangkat Lunak Struktur dan Berorientasi Objek.* Bandung: Information.

LOGIC
Journal of Engineering Design and Technology
Vol. 19 No.3 November 2019; p. 131 - 138

p-ISSN : 1412-114X
e-ISSN : 2580-5649
http://ojs.pnb.ac.id/index.php/LOGIC

THE EKSPERIMENTATION STUDY OF WAVE TRANSMISSION TROUGH TYPE OF HOLLOW CUBE BREAKWATER

Daniel[1], Budiman[2]

1) Head of Work unit PJPA C3 BBWS Banten, Minister for Public Works and Human Settlements , Jl. Ustad Uzair Yachya No. 1 Serang – Banten, Indonesia
2) Lecturer at of Civil Engineering Department, Fakfak State Polytechnic, Jl. TPA Imam Bonjol Atas Air Merah, Kelurahan Wagom Kabupaten Fakfak, Indonesia

Correponding email [2] : budiman@polinef.id

Abstract. Erosion that occurs in break water by wave sand currents is a serious problem along coastal and inland shore [1]. This study aimed to assess the effect of the model height (Hm) and the pole density on the model on the reduction of the wave height and on the relationship between the non-dimensional parameter. The research was experimental with 2D physical model simulation which was conducted in the laboratory of Marine Engineering Faculty, Hasanuddin University. Several of configurations of Hollow-type breakwater models were made with different densities and model heights. The model scale use was 1:10 for the three model variations ((M1KB, M2KB, and M3KB) with the variations of the periods and of the wave height, at 0,25 m water depth. The research results indicated that the parameters which showed significant effects were the model height and the model density. These parameters showed the transmission coefficient (K_t) which tended to decrease while the value of the density and model height tended to increases respectively. The value (Kr) also showed an increased response to the increasing value of ψ. This is consistent with the theory that the closer the structure cross-sectional series to the in-coming waves, the greater the response of the reflection wave height. Hence, the is non regression equation which showed the relationship between the non-dimensional parameter ψ with K_t and K_r, was produced $K_t = m.e^{-n\psi}$ and $K_r = p.\ln\psi + q$ where $\psi = \zeta.\frac{H_i}{L}$; m and n respectively 0,6882 and -4,818; p and q respectively 0,046 and 0,3493.

Keywords : Breakwater Hollow Cube Type, Non-dimentional Parameter (NDP), Transmission Coefficient (K_t)

1. INTRODUCTION

One problem that arises along with the development of coastal areas is the occurrence of coastal erosion. Coastal erosion influenced by natural and non-natural factors. So that the damage to the beach is not getting worse, there needs to be handling, one of which is by making a breakwater which aims to reduce the wave energy so that there is a reduction in energy so that it does not cause damage when the waves arrive on the coast. Breakwater buildings are made to protect the coast from wave attacks that have the potential to cause erosion and also protect certain areas from experiencing sea level fluctuations with short periods [1].

So that the damage to the beach is not getting worse, it needs treatment, one of which is by making a breakwater which aims to reduce the wave energy so that there is a reduction in energy so that it does not cause damage when the waves arrive on the coast [2].

Breakwater structures are designed to protect the coast from wave attacks that have the potential to cause erosion and also protect certain areas from experiencing sea level fluctuations with short periods. Pile of stone breakwater (Rubble mound) is a flexible construction wherein the outermost layer is called layer protection (armor layer) which is useful for protecting breakwaters from wave attack. The use of rubble mound breakwater

in deep waters will certainly cost a very high (not economical) [3].

Various laboratory scale physical model studies have been done before in the coastal protection. Development of a numerical model for calculating reflections of irregular waves for a cascade breakwater with perforations on some of its walls. The numerical model is then verified by testing the physical model in the laboratory [4].

Testing of the perforated breakwater model, where the structure is a massive structure starting from the bottom to the top of the breakwater with the perforation part at the top [5].

The breakwater model consists of impermeable wave barriers that are installed starting on the surface of the water and extended to some distance below the surface of the water [6].

On the basis of the above, the study of wave transmission through hollow cube type breakwater is carried out as an alternative breakwater for coastal protection. Breakwater in question is in the form of hollow cubes that are printed from concrete. To find out the effectiveness of the performance of the above breakwater, an approach is carried out by testing the physical model of hollow cube type breakwater in the laboratory. This reseacrh aimed to assess the effect of the model height (Hm) and density (ζ) pole on the model of the wave height reduction and gain exposure dimensionless parameter.

2. METHODS

2.1 Research Design

This experiment is a physical test in a 2-D wave channel equipped with wave drive with a flume length of 18.45 m, a width of 1.23 m and a height of 1.22 m. At the end of the channel there is a tilted wave absorber that serves to absorb and reduce wave reflection. This research will use a hollow cube with the arrangement of the pillars of concrete molds as a wave barrier that forms a breakwater. Variation model height is 0.125 m, 0.25 m and 0.375 m, while variations in density are 0.68, 0.64 and 0.59. The model scale use was 1:10 for the three model variations ((M1KB, M2KB, and M3KB) and of the wave height, at 0.25 m water depth as shown in table 1.

Table 1. Arrangement of the pillars of concrete molds

Model	Relative Density (ζ)	Model Height (*Hm*)
Model 1	0,68	0,125, 0,25, 0,375
Model 2	0,64	0,125, 0,25, 0,375
Model 3	0,59	0,125, 0,25, 0,375

The series of simulations performed in this study is to place a hollow cube type breakwater model in the center of the flume equipped with a measuring instrument in front of and behind the model and then the wave is generated as shown in Figure 1 and 2. Simulation parameters consist of density (ζ), model height (Hm), water depth (d). While the parameters observed were the incident wave height (Hi), wave reflection (Kr), wavelength (L), density of each model (ζ), model height (Hm) and wave transmission (Kt).

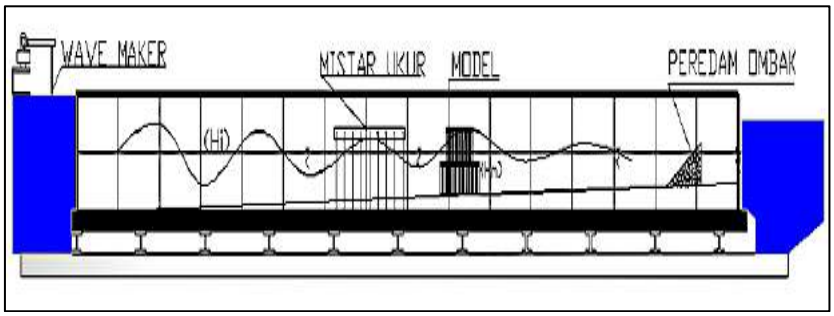

Figure 1. Wave channel 2-D

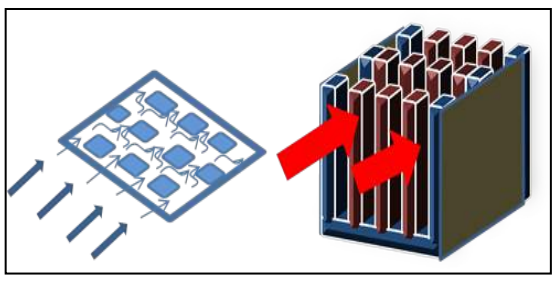

Figure 2. Model sketches

Model simulation procedure is as follows:

1. Perform equipment calibration (setting pulleys for periods and wavelengths, strokes for height and fast wave propagation, and setting the position of breakwater hollow cubes) for recording wave heights (H).
2. After the component is ready, the wave simulation starts without a model by generating waves with power levers on the wave generator control.
3. Then proceed to install the model in the middle of the wave flume
4. The height of the incident wave is measured in front of the position of the model at 9 points
5. Procedures 1 to 5 continue repeatedly on the other models for each model, with variations in density, number of layers, distances, stroke parameters for wave height, fully for the wave period and fixed water depth.

2.2 Research Stages

The stages of the research can be seen in Figure 3.

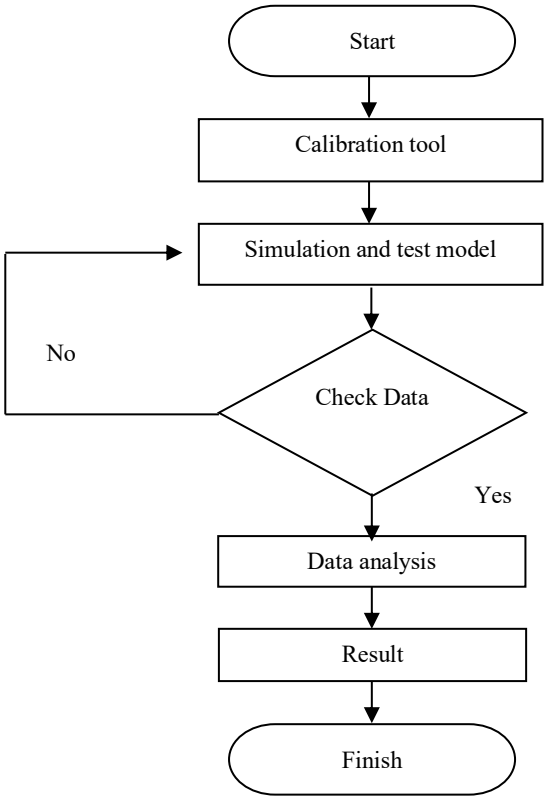

Figure 3. Flowchart of research stage

2.3 Dimension analysis

The data obtained is processed using dimensional analysis to obtain relationships between parameters that will produce dimensionless numbers. The dimension analysis method used in this study is the Langhaar method [7].

Dimensionless number (πj) can be stated:

$$\pi_j = P_1^{k1} P_2^{k2} P_3^{k3} \ldots\ldots\ldots\ldots P_n^{kn} \quad (1)$$

Where πj = product of dimensionless numbers with j = 1, 2, 3, ... n. if Pi has dimensions $M^{\alpha i}$, $L^{\beta i}$, $T^{\gamma i}$, then it can be written:

$$\pi_j = \left(M^{\alpha 1k1+\alpha 2k2+\ldots+\alpha nkn}\right) * \left(L^{\beta 1k1+\beta 2k2+\ldots+\beta nkn}\right) * \left(T^{\gamma 1k1+\gamma 2k2+\ldots+\gamma nkn}\right) \quad (2)$$

πj is a dimensionless number if:

$$\alpha_1 k_1 + \alpha_2 k_2 + \ldots\ldots\ldots + \alpha_n k_n = 0$$
$$\beta_1 k_1 + \beta_2 k_2 + \ldots\ldots\ldots + \beta_n k_n = 0$$
$$\tau_1 k_1 + \tau_2 k_2 + \ldots\ldots\ldots + \tau_n k_n = 0 \quad (3)$$

3. RESULTS AND DISCUSSION

3.1 Wave Height (Hi), Transmission (Ht) and Reflection (Hr)

The recording of incident wave height (Hi), transmission (Ht) and reflection (Hr) of the experiments in the 2-D Laboratory at each observation point were taken from the maximum value of Hmax and the minimum wave height of Hmin. The transmission wave height (Ht) is the same as the incident wave height (Hi) but the transmission wave occurs behind the model. The waves came the about / hit an obstacle will be reflected in part the so-called reflection wave height (Hr) as shown for example in table 2.

Table 2. Results of the calculations Hi, Ht, and Hr by high variation models (Hm) and density models (ζ)

Type model	St	ζ	Hm	Wave lenght (L) (cm)	Hi (cm)	Ht (cm)	Hr (cm)
M1KBL1, T= 1,003	St1		12,5	130,928711	7,50	4,50	2,50
M1KBL1, T= 1,025	St2	0,68	12,5	134,909991	6,75	4,75	1,75
M1KBL1, T= 1,048	St3		12,5	139,052187	6,25	4,00	1,75
M2KBL1, T= 1,003	St1		12,5	130,928711	8,50	4,50	2,50
M2KBL1, T= 1,025	St2	0,64	12,5	134,909991	7,50	4,00	2,50
M2KBL1, T= 1,048	St3		12,5	139,052187	7,00	3,75	2,00
M3KBL1, T= 1,003	St1		12,5	130,928711	7,50	3,75	2,50
M3KBL1, T= 1,025	St2	0,59	12,5	134,909991	6,50	3,50	2,50
M3KBL1, T= 1,048	St3		12,5	139,052187	6,00	3,25	2,00

3.2 Transmission Wave Coefficient (Kt) and Reflection (Kr)

The comparison between transmission wave height (Ht) and incident wave height (Hi) is called the transmission coefficient (Kt). The comparison between the reflection wave height (Hr) and the incident wave height (Hi) is called the reflection coefficient (Kr). The amount of wave energy destroyed / muted is called the dissipation coefficient (Kd), for example as in table 3.

Table 3. The results of Kt and Kr calculations are based on variations in model height and model density (ζ)

Type model	St	ζ	Hm	Wave lenght (L) (cm)	K_t	K_r	K_d
M1KBL1, T= 1,003	St1		12,5	130,928711	0,58	0,33	0,09
M1KBL1, T= 1,025	St2	0,68	12,5	134,909991	0,58	0,26	0,14
M1KBL1, T= 1,048	St3		12,5	139,052187	0,64	0,28	0,08
M2KBL1, T= 1,003	St1		12,5	130,928711	0,53	0,29	0,18
M2KBL1, T= 1,025	St2	0,64	12,5	134,909991	0,53	0,33	0,16
M2KBL1, T= 1,048	St3		12,5	139,052187	0,54	0,29	0,12
M3KBL1, T= 1,003	St1		12,5	130,928711	0,50	0,33	0,17
M3KBL1, T= 1,025	St2	0,59	12,5	134,909991	0,54	0,38	0,12
M3KBL1, T= 1,048	St3		12,5	139,052187	0,54	0,33	0,13

3.3 Effect of NDP = (Hi / L) on Kt and Kr

Effect of wave parameters on the transmission coefficient (Kt) and reflection coefficient (Kr) used the dimension of the wave steepness dimensionless. The steepness of the wave (Hi / L) with respect to Kt and Kr for the simulation model height (Hm) and Model Density (ζ) as shown in Figure 4 and 5.

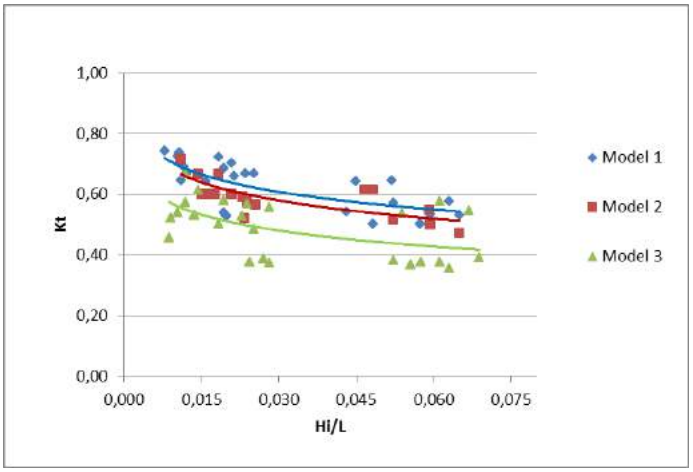

Figure 4. Relationship of Hi / L to Kt based on variations model height (Hm) and model density (ζ)

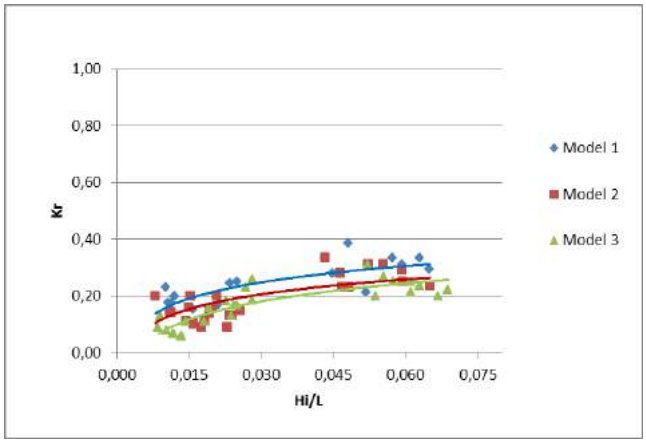

Figure 5. Relationship of Hi / L to Kr based on variations model height (Hm) and model density (ζ)

Based on Figure 4 and 5, shows the value of Kt has decreased significantly with the increasing value of Hi / L. Vice versa for the value of Kr has increased significantly. The change is influenced by the structure density of the model that is able to reduce the waves to be transmitted, as well as to reflect the waves again as the wave steepness that hits the structure increases.

3.4 Effect of NDP = $\zeta.\frac{H_i}{L}$ on K_t and K_r

Analysis of the relationship between the transmission coefficient (Kt) and the reflection coefficient (Kr) with $\zeta.\frac{H_i}{L}$ with a variety of relative and high density models to determine the effectiveness and influence of the characteristics of the model being made. The relationship ψ with the transmission coefficient (Kt) and reflection coefficient (Kr), where $\psi = \zeta.\frac{H_i}{L}$ as the X and Kt axis variables, Kr as the Y axis variable for each type of model, an graph is produced which is an exponential graph as in Figure 6 and 7 (based on the theory "If both progressive and standing waves propagate through an axis media, then the amplitude of the waves will decrease exponentially" [8].

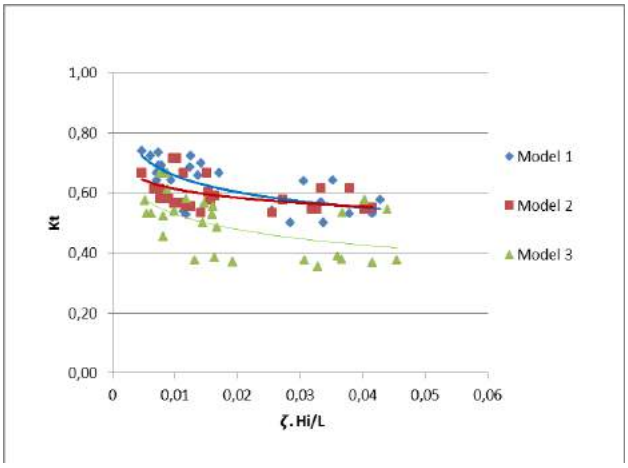

Figure 6. Relationship $\zeta.\frac{H_i}{L}$ with Kt for 3 variations in density and model height.

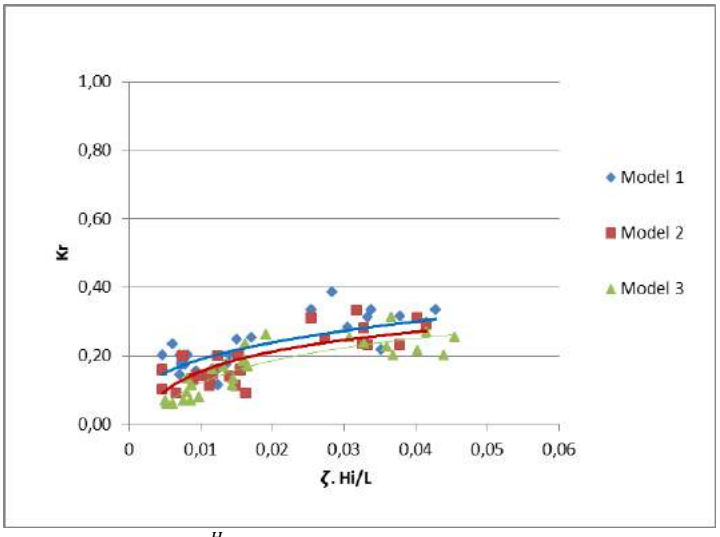

Figure 7. Relationship $\zeta.\frac{H_i}{L}$ with Kr for 3 variations in density and model height.

Based on Figure 6 and 7 for the type of model with variations in relative density and height of the model shows an influence on the steepness of the wave (Hi / L). The greater the density and height of the model, the greater the steepness of the wave so that the transmitted wave gets smaller and the greater the reflected wave.
If all the combined data is plotted in graphical form showing the relationship between ψ and the transmission coefficient (Kt) and the reflection coefficient (Kr) as in Figure 8 and 9.

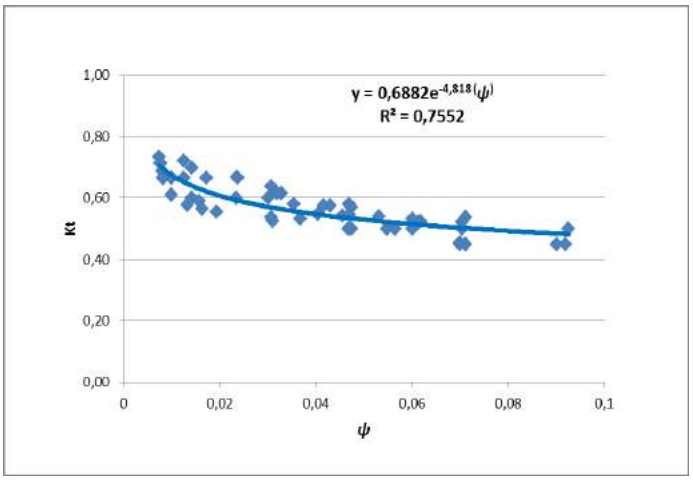

Figure 8. Relationship ψ with K_t

Figure 8 shows that the greater the value ψ the smaller the value of the transmission coefficient (Kt). This is in accordance with the theory, where the height of the wave that passes through an obstacle will decrease non-linear (exponential) with a reduced value of the smaller wave height. This experiment produces an equation of the dimensionless parameter relationship between ψ and Kt.

$$Kt = \frac{Ht}{Hi} = m.e^{-n\psi} \quad (4)$$

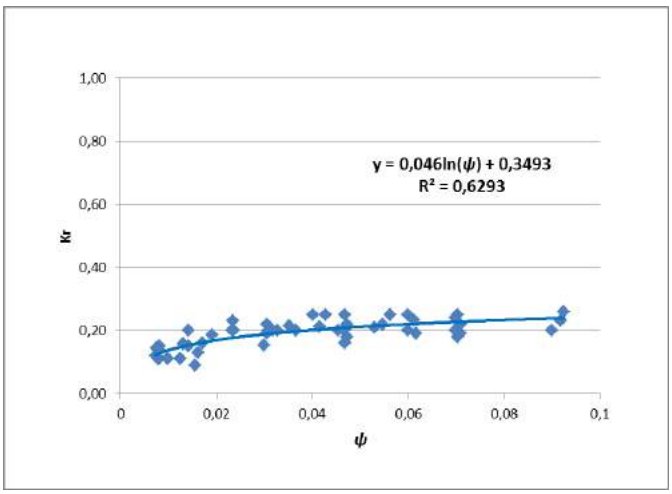

Figure 9. Relationship ψ with K_r

Figure 9 shows the greater the value ψ the Kr value also increased by a significant increase gradient. This is in accordance with the theory, where the closer the cross-section of the model that is subjected to a coming wave, the higher the wave height is reflected by the dimensionless parameter relation equation

$$Kr = \frac{Hr}{Hi} = p.ln\psi + q \quad (5)$$

Where :

Kt = wave transmission coefficient, Hi = coming wave height

Kr = wave reflection coefficient, Hr = reflection wave height

Ht = transmission wave height, Ψ = the Hollow Cube friction parameter = $\zeta.\frac{H_i}{L}$

ζ = density of hollow cube poles, L = wavelength

m and n = constants with values 0.6882 and -4.818, p and q = constants with values of 0.046 and 0.3493. In order to obtain the regression equation for the values of Kt and Kr.

$$K_t = 0{,}6882\, e^{-4{,}818\,(\psi)} \quad \text{with } R^2=0{,}7552 \quad (6)$$

$$K_r = 0{,}046 \ln(\psi) + 0{,}3493 \quad \text{with } R^2=0{,}6293 \quad (7)$$

The equation obtained can then be used for planning the wave damping structure using a hollow cube type breakwater structure.

Based on the analysis and dimensionless relationship between the friction parameter (ψ) of the transmission coefficient (Kt) and the reflection coefficient (Kr), where the higher the value of ψ, the lower the value of Kt and the increasing value of Kr. The greater the value of Hi / L (increasingly steep waves) are the model of the Kt value tends to decrease, height models (Hm) also affect the high reduction of the wave through the transmission coefficient, where the higher the model, it tends to be the smaller the value Kt.

As well, the effect of pole density on the hollow cube model (ζ), where the closer the cube poles to the wavelength, the smaller the value of Kt. The effectiveness level of perforated skirt breakwater (PSB) in the long wave category shows the greater the draft breakwater (s), the smaller the transmission coefficient (Kt).

Whereas with the increase in value Kr, the value of Kr also increases with a significant increase in gradient. This is consistent with the theory, where high waves that pass hurdle will be reduced non-linear (exponential) with high reduction value of the smaller waves. A wave damper structure can also be said to be good if the reflection wave thereof is small enough so as not to adversely impact the area in front of it [1]. The same thing was expressed [8], if both progressive and standing waves propagate through a pivot media, the amplitude of the waves will decrease exponentially. Wave transmission depends on the depth of the barrier both at the front and rear of the breakwater while the wave reflection depends on the depth of the barrier at the front of the breakwater [6].

4. Conclusion and suggestion

4.1 Conclusion

Based on the results of research and data analysis that has been implemented, it can be concluded some points as follows:

1. The height of the model has a significant effect on the transmission coefficient (Kt) and the reflection coefficient (Kr), where the greater the value of Hm or the higher the model, the smaller the value of Kt and the greater the value of Kr. Similarly, the pole density ζ models affect the Kt and Kr, where the meeting of the pillars on the model of the transmission coefficient (Kt) is getting smaller and the reflection coefficient (Kr) increases.
2. The research of testing the hollow cube type breakwater model in the Laboratory obtained a dimensionless relationship between the friction parameter (ψ) of the transmission coefficient (Kt) and the reflection coefficient (Kr), where the higher the value of ψ, the lower the value of Kt and the increasing value of Kr and have the equation $K_t = m.e^{-n\psi}$ and $K_r = p.ln\psi + q$, where $\psi = \zeta.\frac{H_i}{L}$; m and n respectively 0,6882 dan -4,818; p and q respectively 0,046 dan 0,3493.

4.2 Suggestion

Based on the conclusion, the suggestion or recommendation from this research is as follows:

1. This research uses 2-D channels made of steel, so it is recommended to use 2-D channels made of glass, in order to facilitate the observation of data
2. This research did not carry out numerical validation of the hydrodynamic characteristics of the breakwater types.
3. Further research needs to be done with variations in the depth of the water in the channel

5. ACKNOWLEDGEMENT

Acknowledgement is given to the marine civil engineering University Hasanuddin for permission to use the Hydrodynamics Laboratory facilities

6. REFERENCES

[1] Triatmodjo, Bambang. 1999. *Teknik Pantai*. Beta Offset. Yogyakarta.
[2] Sorensen, R.M. 2006. *Basic Coastal Engineering, Third Edition*. Springer Science+Business Media, Inc. New York.
[3] Defiana, Yanti. 2006. *Transmisi Gelombang Melalui Beton Ringan Styrofoam Sebagai Pemecah Gelombang Terapung*. Tesis tidak diterbitkan. Yogyakarta: Program Pascasarjana UGM.
[4] Suh, Kyung-Duck. Park, Jae Kil. dan Park, Woo Sun. 2006. Wave Reflection from Partially Perforated-Wall Caisson Breakwater. *Ocean Engineering*, (Online), Vol. 33, (http://coasteng.snu.ac.kr /thesis/ij06a.pdf, diakses 12 Maret 2011).
[5] Ariyarathne, H.A.K.S. 2007, *Efficiency of Perforated Breakwater and Associated Energy Dissipation*. Tesis dalam format elektronik. Office of Graduate Studies of Texas A&M University. USA.
[6] Laju, Kottalil. Sundar, Vallam. dan Sundaravadivelu, R. 2005. *Studies on Pile Supported Skirt Breakwater*. Paper disajikan pada 1st International Conference on Coastal Zone Management and Engineering in the Middle East (Arabian Coast), Habtoor Grand Jumeirah Beach, Dubai, Uni Emirat Arab 27-29 November 2005.
[7] Yuwono, Nur. 1996. *Perencanaan Model Hidrolik (Hydraulic Modelling)*. Laboratorium Hidrolik dan Hidrologi, Pusat Antar Universitas Ilmu Teknik-UGM. Yogyakarta.
[8] Dean dan Dalrymple. (1992). *Water Waves Mechanics for Engineers and Scientists*.World Scientific Publishing. Singapore.

LOGIC
Journal of Engineering Design and Technology
Vol. 19 No.3 Nopember 2019 ; p. 139 - 144

p-ISSN : 1412-114X
e-ISSN : 2580-5649
http://ojs.pnb.ac.id/index.php/LOGIC

DESIGNING AND MANUFACTURING THE PRESS TOOL OF AIR BENDING V BRAKE

Rusdi Nur[1)], Muhammad Arsyad Suyuti[2)], Muhammad Iswar[3)]

1,2,3) Politeknik Negeri Ujung Pandang, Jl. Perintis Kemerdekaan Km. 10 Tamalanrea Makassar

Correponding email [1)] : rusdinur@poliupg.ac.id

Abstract. Nowadays, the metal forming process in the welding machinery and machinery industry is developing very rapidly, especially in the bending process. The buckling process is a metal formation which generally uses sheet plates or rods from both ferrous and non-ferrous metals by bending, which in the bending process will cause a stretching or stretching on the neutral axis of the field along the bending area and producing a straight bending line. Appropriate technology machines have been widely used to increase productivity, efficiency, and effectiveness in the production process for community efforts. One of the appropriate technologies that can be applied in buckling is a tool equipped with a press tool. Press tool is one type of tool for the formation, cutting and bending of products from the base material of sheet plates whose operation uses a press machine. This paper have several stages, such as: designing consept, manufacturing product, assembling, and testing the press tool. In this study, a V brake bending tool has been produced which has a capacity that is bending line length 300 mm, bending width 33 mm, spring height 110 mm, free step distance 19 mm, spring load received 263,820 N and material capacity that can be bent is a thickness of 3 mm, the punch angle used is 85º with a punch radius used which is 1.5 mm while the die angle is 85º

Keywords : press tool, air bending, design and manufacture.

1. INTRODUCTION

The metal forming industry has developed very rapidly, especially in the bending process especially in the machinery and welding workshop industry. The buckling process is a metal formation that generally uses sheet plates or rods from both ferrous and non-ferrous metals by bending, which in the bending process will cause a stretching or stretching on the neutral axis of the field along the bending area and producing a straight bending line [1][2]. The phenomenon of the development of metal formation through buckling processes occurs in the manufacturing industry in large cities in large-scale and small-scale welding machinery and workshops in rural areas. This was triggered by the increasing use of various kinds of mechanization technology, especially in the field of food security and security in everyday people's lives such as post-harvest process technology and other agricultural mechanization technologies. [3][4].

Several buckling processes are often carried out in the manufacturing process for the manufacture and repair of products in machinery and welding manufacturing workshops such as electronic panel components, automobile vehicle panels, toolboxes, fish combustion, agricultural machinery, and mechanization tools and so on. However, there are still many small-scale workshops that bend the plates manually, namely using a hammer and iron base as a base so that the time used is not efficient and the resulting product is not guaranteed quality. Equipment owned by industry is usually a large-capacity engine where operational costs will be large while producing small-sized objects does not have to use large-capacity machines. Because of that, small plate bending tools are needed.

Thus, the application of appropriate technology is needed to increase the effectiveness of metal formation through this bending process. The use of appropriate technology machines has been widely used to increase

productivity, efficiency, and effectiveness in the production process for community businesses, especially those in the area. One of the appropriate technologies that allow it to be applied in buckling is a press machine equipped with a press tool.

Press tool is one type of tool for the formation, cutting and bending of products from the base material of sheet plates whose operation uses a press machine. Based on its formation process the Press tool is clarified into three, namely coining, bottoming and water bending. Formation using coining and bottoming is more accurate but to require different bending angles, it must use a different punch and die. Unlike the case with metal formation using water bending, to produce different bending angles only need to use one punch and die and different emphasis steps [5] [6].

2. METHODS

This research was carried out in the mechanical workshop and mechanical laboratory of Ujung Pandang State Polytechnic. The materials used in this study included iron shaft St 42, US box St 42, and steel plates. While the equipment used is milling machines, lathes, drilling machines, grinding machines, cutting saw machines and various dimensional measuring instruments. Several stages are carried out in this design so that it can run well, namely:

Firstly, the design stage begins by designing the press concept V bending tool that will be created. The concept of this design is continued by making image design in accordance with ISO standards. This image design includes the overall design drawing design and image design for all components both components made and standard components.

Secondly, in manufacturing and assembly stage, the nonstandard components are made by referring to the working drawings of the design. while standard components are purchased. After all the components that have been made and purchased are finished, a press tool assembly is carried out based on the results of the design.

Lastly, the press tools that have been assembled are then tested by bending the plates of low carbon steel. The trial process is carried out using 85o angle V-shaped dies. While the punch used is an 85º angle and a 1.5 mm radius. After the trial is completed, the resulting product is then measured by its bending angle to obtain. The sheet base material used is the St 37 carbon steel plate with a thickness of 3 mm.

3. RESULTS AND DISCUSSION

3.1 Result of Designing Press Tool

The press tool component consists of die sets, punch and dies themselves. Die set is a stand for assembling all components of the press tool. Die sets designed to be used as a tool to bend the plate material from carbon steel. This die set is specifically designed so that the punch and dies can be changed according to needs.

A. Designing the Construction of Press Tool

The design of the die set auxiliary construction along with the punch and die that will be used is as follows:

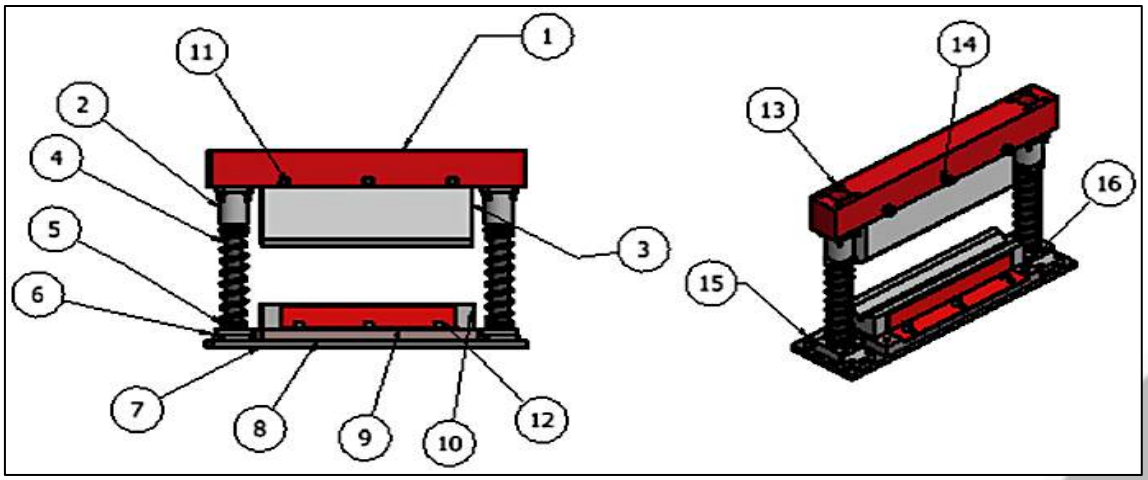

Figure 1. Design construction of press tool

Based on Figure 1, the press tool consists of several components, namely: 1) Top Plate; 2) Bearing; 3) Punch; 4) Spring; 5) Shaft; 6) Axle Stand; 7) Bottom Plate; 8) Coating plates; 9) die locking plate; 10) die; 11) Punch and Top Plate Binder Bolts; 12) Die locking bolt; 13) Bolt Bearings; 14) Punch and Top Plate Binding Nuts; 15) Holder bolt; 16) Die Coating Bolts.

B. Calculating the Construction of Press Tool

Some components play an important role in the V Brake bending process. Therefore, it is necessary to do some calculations to get the right design results as follows:

1. Loading for Load Spring. Die set components to provide spring load, namely top plate, punch, ring, and bearing. The determination of the mass of the die set auxiliary tool which is spring-loaded is used the equation as follows [7]:

$$W = V.\rho \quad (1)$$

Where W is component mass (kg), V is component volume (mm^3), ρ is density (kg/mm^3). Making components was using medium carbon steel density of 7860 Kg / m3. The following is a calculation of the mass of components that overload the spring:

a. Mass of Top plate (W_{tp}) = (Vtot . ρ)
= (V_I - V_{II} - V_{III} - V_{IV}) . ρ
= 11,407 kg

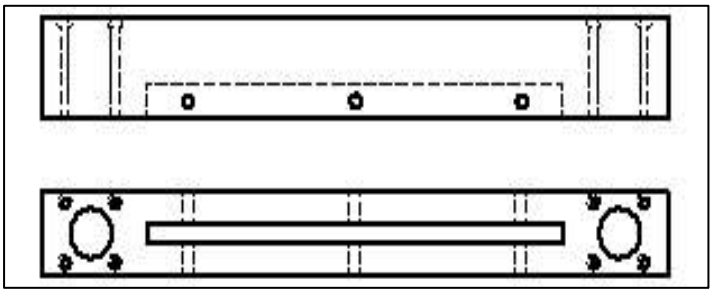

Figure 2. Top plate

b. Mass of Punch (Wp) = (Vtot . ρ)
= (V_I - V_{II} + V_{III} + V_{IV}) . ρ
= 15,339 kg

c. Mass of Bearing (Wb) = 2,377 kg (stainless steel)

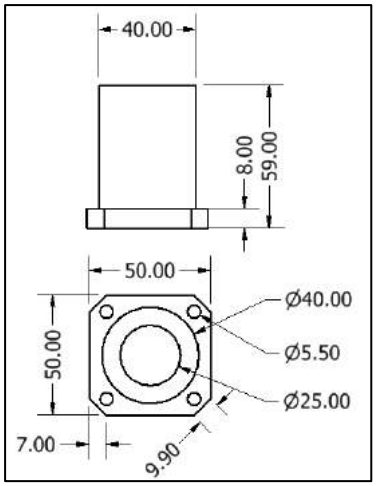

Figure 3. Bearing

d. Mass of Ring (Wr) = 0.046 kg (brass)

Thus, the total load received by the spring is:

$W_{total} = W_{top\ plate} + W_{punch} + W_{bearing} + W_{ring} = 29{,}17kg$

2. Strength of spring. Calculation of spring strength needs to be done to find out the selected spring can return the top plate, punch, and bearing at its original position after loading the bending process is

carried out. It is known that the spring diameter and wire diameter are 40 mm and 5 mm respectively, and the shear modulus (G) = 83x103 N / mm. Then the equation used is as follows [8]:

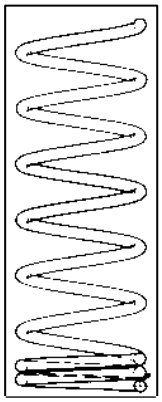

Figure 3. Spring

$$W = \frac{\delta.G.d^4}{8.D^3.n} \quad (2)$$

$$W = \frac{(Lo-Li).G.d^4}{8.D^3.n}$$

$$W = \frac{(110-100).83x10^3.5^4}{8.40^3.2} = 506{,}592 \text{ N}$$

There are 2 pieces of springs on the die set, the load that is able to be retained by the spring theoretically is 1,013,184 N. Based on the calculation of the total load of the upper component of the die set received by the spring (Wtot) of 29.17 kg or 263,820 N, then springs used are safe because the spring load is greater than the total load received

C. Result of manufacturing Press Tool

In this study, the design and manufacture of press tools produced one die set which was equipped with one punch with an angle of 85^0 1.5 mm radius and or V-shaped fruit dies at an angle of 85^0. This press tool is capable of bending product components and machining of various metal sheet materials precisely. Bendable components have a maximum width of 300 mm. The press tool that is produced can be seen in Figure 4.

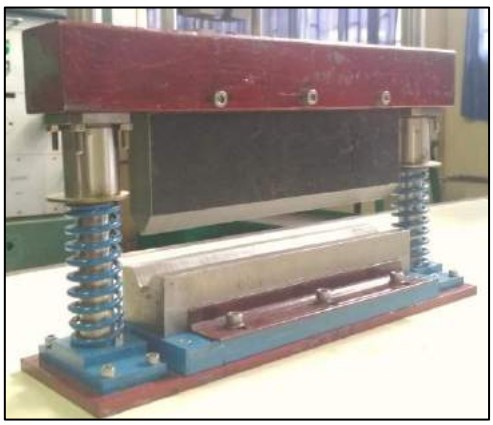

Figure 4. Press tool die set

3.2 Result of Testing Press Tool

After the assembly process is complete, the next step is to test the press tool to find out whether the tool is functioning properly or not. The trial process can be seen in Figure 5.

Figure 5. Press tool die set on UTM (Universal Testing Machine)

In this testing process, 10 test samples were carried out with the punch angle used, namely 85º radius 1.5 mm, dies with the angle used 85º and the material to be tested was St 37 carbon steel thickness of 3 mm. The results of testing the press tool measuring 300 x 60 x 3 mm from St 37 steel thickness 3 mm can be seen in Figure 11 as follows:

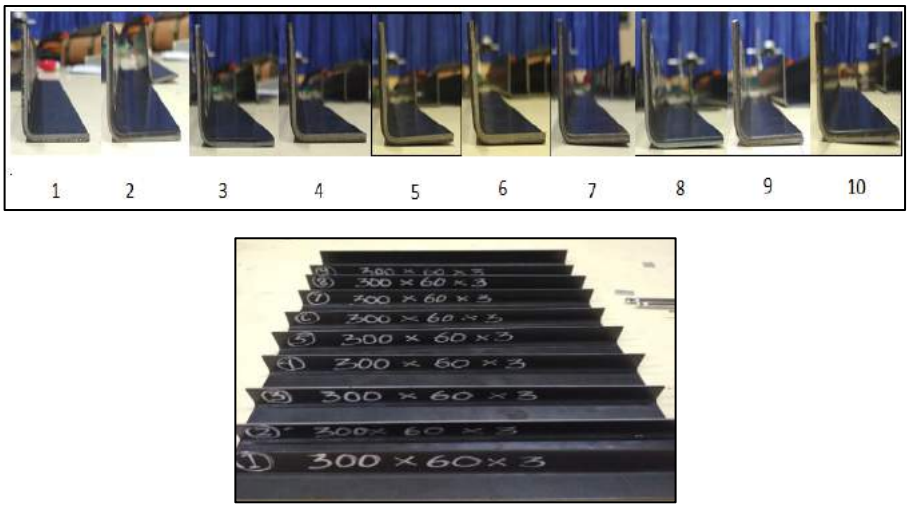

Figure 6. Product of testing press tool

The data on the measurement of bending angle from the press brake tool V brake can be seen in Table 1 below.

Table 1. Test Results Data Press Tool V Brake Bending tool

No.	Load (N)	Bending Angle			Springback
		(º)	(")	(º)	(º)
1	395	90	15	90,25	5,25
2	349	90	25	90,42	5,42
3	345	90	30	90,5	5,5
4	349	91	0	91	6
5	342	89	30	89,5	4,5
6	342	91	0	91	6
7	349	90	45	90,75	5,75
8	355	90	0	90	5
9	343	90	5	90,08	5,08
10	345	90	15	90,15	5,15

Based on the table above shows that all bending angles produced are close to 90º and 90º, and springback is close to 5º and 5º. The bending angle produced is equal to 90º and springback is equal to 5º located at test

number 8. While the bending and springback angle deviations are greatest with the bending angle 91, and the same springback 6 value is in the test numbers 4 and 6.

3.3 Discussion

The results of the design and manufacture of press tool has been done well. This press tool has also been tested with bending of sheet metal. The design and manufacturing model has also been done by Suyuti et al who made a simple press tool for V-bending bottoming [9], as well as designing the prototype of a press tool for making an O-ring with pneumatic System [10].

4. CONCLUSION

Based on the results of the study, it can be concluded that the results of designing and manufacturing the Air Bending V Brake Press Tool can be used as a tool for bending production V. The specifications of this V Brake Air Bending Press Tool are bending line length 300 mm, bending width 33 mm, spring height 110 mm, free step distance of 19 mm, spring load received 263,820 N and capacity of material that can be bent is ST 37 thickness 3 mm.

5. ACKNOWLEDGEMENT

The author sincerely thanks Ministry of Research and Technology of Higher Education for funding the superior university applied research (PTUPT-DIKTI) and Ujung Pandang State Polytechnic for supporting the research.

6. REFERENCES

[1] W. F. Hosford and R. M. Caddell, *Metal forming: mechanics and metallurgy*. Cambridge University Press, 2011.
[2] F.-K. Chen and S.-F. Ko, “Deformation analysis of springback in L-bending of sheet metal,” *Advanced Science Letters*, vol. 4, no. 6–7, pp. 1928–1932, 2011.
[3] A. S. Muhammad and N. Rusdi, “The Effect of Embossing on the Rigidity of Wheel for Agricultural Tractors.” Research Institute and Community Services University of Lampung, 2016.
[4] M. A. Suyuti, “Rancang Bangun Prototipe Alat Metal Forming Sirip Roda Besi Traktor Tangan,” *Jurnal Sinergi Jurusan Teknik Mesin*, vol. 13, no. 1, pp. 62–74, 2019.
[5] T. Altan and A. E. Tekkaya, *Sheet metal forming: processes and applications*. ASM international, 2012.
[6] K. Osakada, K. Mori, T. Altan, and P. Groche, “Mechanical servo press technology for metal forming,” *CIRP annals*, vol. 60, no. 2, pp. 651–672, 2011.
[7] R. Nur and M. A. Suyuti, *Perancangan mesin-mesin industri*. Deepublish, 2018.
[8] V. B. Bhandari, *Design of machine elements*. Tata McGraw-Hill Education, 2010.
[9] M. A. Suyuti, “Rancang Bangun Simpel Press Tool untuk Bending V Bottoming,” *Jurnal Sinergi Jurusan Teknik Mesin*, vol. 13, no. 2, pp. 160–173, 2019.
[10] P. Gautama, S. Ka’ka, M. A. Suyuti, and T. A. Susanto, “Desain Prototipe Alat Press Tool untuk Pembuatan O-Ring Sistem Pneumatik,” *Jurnal Sinergi Jurusan Teknik Mesin*, vol. 12, no. 2, pp. 114–123, 2019.

LOGIC
Journal of Engineering Design and Technology
Vol. 19 No.3 November 2019; p. 145 - 154

p-ISSN : 1412-114X
e-ISSN : 2580-5649
http://ojs.pnb.ac.id/index.php/LOGIC

BEARING CAPACITY ANALYSIS OF BRIDGE FOUNDATION BASED ON CONE PENETRATION TEST DATA AND SOIL PARAMETERS DATA

A CASE STUDY: AIFA BRIDGE IN FAFURWAR DISTRICT, BINTUNI BAY REGENCY WEST PAPUA PROVINCE

Muhammad Yunus [1)], Zharin F. Syahdinar[2)]

1, 2) Civil Engineering Department, Polytechnic State of Fakfak

Jl. TPA Imam Bonjol Atas Air Merah Wagom Village, Fakfak Regency, West Papua Province

Phone : +628114212748

Correponding email [1)] : muhammadyunus@polinef.id

Abstract. The aim of this research to test characteristics of the soil and calculate bearing capacity of the foundation based cone penetration testing data and soil parameters at the Aifa bridge construction field in Fafurwar District, Teluk Bintuni Regency, West Papua Province. Research carried out with survey the construction site of the bridge and conduct a sondir test in accordance with the location of the bridge abutment according to the bridge design drawings. Along with the implementation of sondir test, soil sampling is carried out to be taken to the laboratory for soil characteristics testing. Soil parameter testing carried out in the laboratory, among others, water content test, specific gravity test, unit weight test, Atterberg limit test, soil grain size test, compaction test and shear strength test. From the results of testing the soil characteristics in the laboratory, the type of soil at point 1 is the type of good to bad graded sand soil (SW-SP) with a water content of 17.72%, specific gravity 2.98, liquid limit (LL) = 16,746% included in the non-plastic category. While the location of point 2 is obtained from good to bad graded sand soil type (SW-SP) with a water content of 28.52%, specific gravity 2.73, liquid limit (LL) = 16.746% including the non-plastic category. To analysis of the calculation of the bearing capacity of the foundation Aifa bridge using data from the sondir test results for point 1 was obtained allowable bearing capacity (Q_{all}) is 4.610,44 kN and for point 2 was obtained allowable bearing capacity (Q_{all}) is 3.598,43 kN. For calculating bearing capacity of the foundation using soil parameter data for point 1 was obtained bearing capacity allowable (Q_{all}) is 2.209,93 kN and for point 2 was obtained allowable bearing capacity (Q_{all}) is 655,41 kN

Keywords : Bearing Capacity, Caisson Foundation, Cone Penetration Testing, Soil Parameter

1. INTRODUCTION

The bridge is one of the important infrastructures in people's lives, because aside from being a link to facilitate transportation between two or more regions separated by rivers and valleys [9]. With a bridge, it can indirectly increase the economic growth of a region.

Bridges have 2 (two) parts, namely the superstructure and the substructure [1], [2]. The upper building is a construction that is directly related to the traffic loads that work [2]. Whereas the lower building is a construction that receives loads from the upper building and passes it on to the supporting hard soil layer below. Bridges that are built must have a high level of security and comfort for the wearer so that they can avoid unwanted events [2].

To build a safe bridge including the bridge must have a strong foundation. The bridge foundation comprises several types, one of which is the caisson foundation that will be used for bridge planning in Fafurwar District, Teluk Bintuni Regency, West Papua Province.

A common problem that is often encountered in bridge construction is the occurrence of structural failures, especially in the lower part of the bridge such as the existence of cracks or damage to the bridge abutment that results in overloading experienced by the foundation, a large decrease in the bridge foundation which over time can result structural failure [3].

To minimize the occurrence of structural failures in bridge construction, especially in the lower part of the building, so when the bridge planning work is needed data of soil parameters around the bridge construction site [6], [7]. To get adequate soil parameters, it is necessary to conduct soil tests in the field such as SPT (Standard Penetration Test) and CPT (Cone Penetration Test) [10] and tests conducted in laboratories such as testing specific gravity, soil volume weight, Atterberg limit, analysis of soil grain size, and shear strength soil [5], [11].

After the results of testing the soil characteristics are carried out, one of the main tasks that the planners need to do is calculate or analyze the bearing capacity of the foundation used in bridge planning. To calculate or analyze the bearing capacity of the foundation especially the caisson foundation, we can do it using empirical methods by using soil parameters data that have got and using data from the CPT (Cone Penetration Test).

2. METHODS

In general, the sequence of work steps taken in this study is as shown in Figure 1.

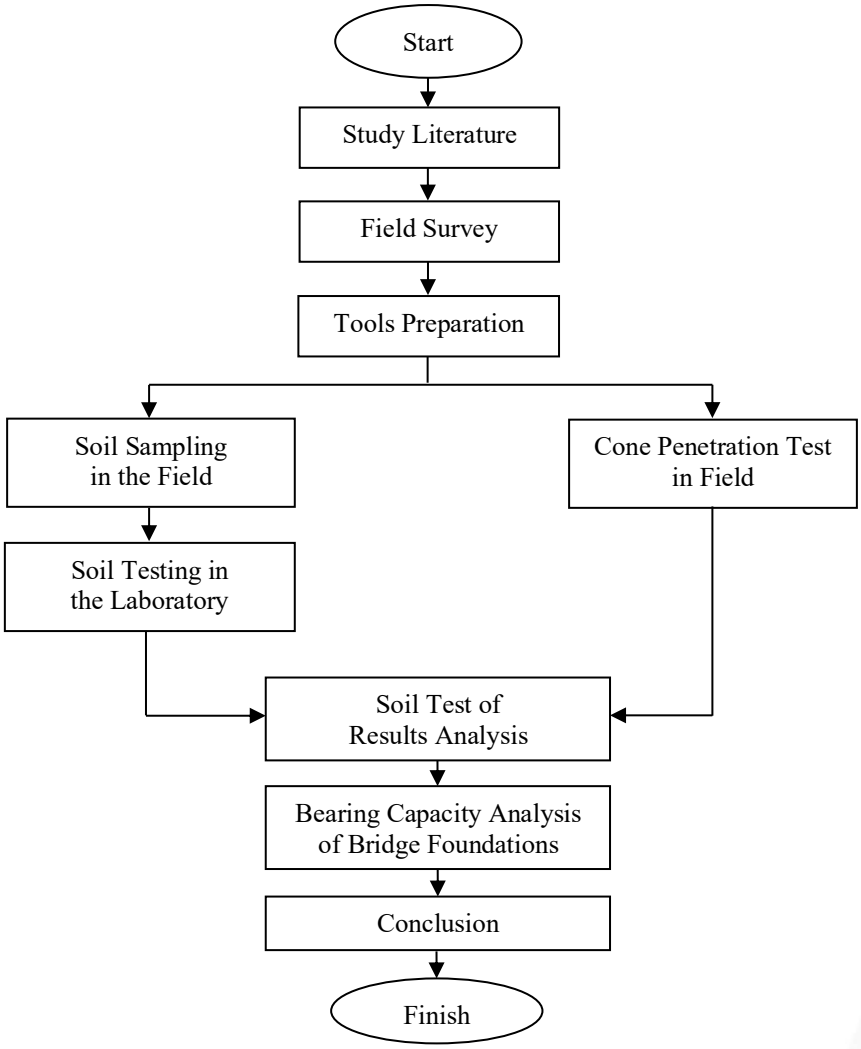

Figure 1. Flowchart of The Research Method

Based on the research flow diagram, the task of the compiler and members of the research is to survey the construction site of the bridge and conduct a sondir test in accordance with the location of the bridge abutment according to the bridge design drawings. Along with the implementation of sondir test, soil sampling is carried out to be taken to the laboratory for soil characteristics testing. Soil parameter testing carried out in the laboratory, among others, water content test, specific gravity test, unit weight test, Atterberg limit test, soil grain size test, compaction test and shear strength test. After the soil parameter data is known from the test results, an analysis of the carrying capacity of bridge foundations uses the type of well foundation (caisson) for construction. Calculation of the carrying capacity of the pitting foundation is divided into 2 (two) types, namely the calculation of the end resistance of the foundation (end bearing, Q_p) and the friction resistance (friction, Q_s). From the calculation of the Q_p and Q_s values, we can determine the ultimate bearing capacity (Q_{ult}) and allowable bearing capacity of the foundation (Q_{all}).

3. RESULTS AND DISCUSSION

3.1 Detail Engineering Design Aifa Bridge

Detail Engineering Design Aifa obtained from the agency Ministry of Public Works of the Directorate General of Highways (BPJN XVII Manokwari). For layout drawing, long section and cross section of the Aifa bridge in Fafurwar District, Bintuni Bay Regency can be seen in Figure 2 annd Figure 3.

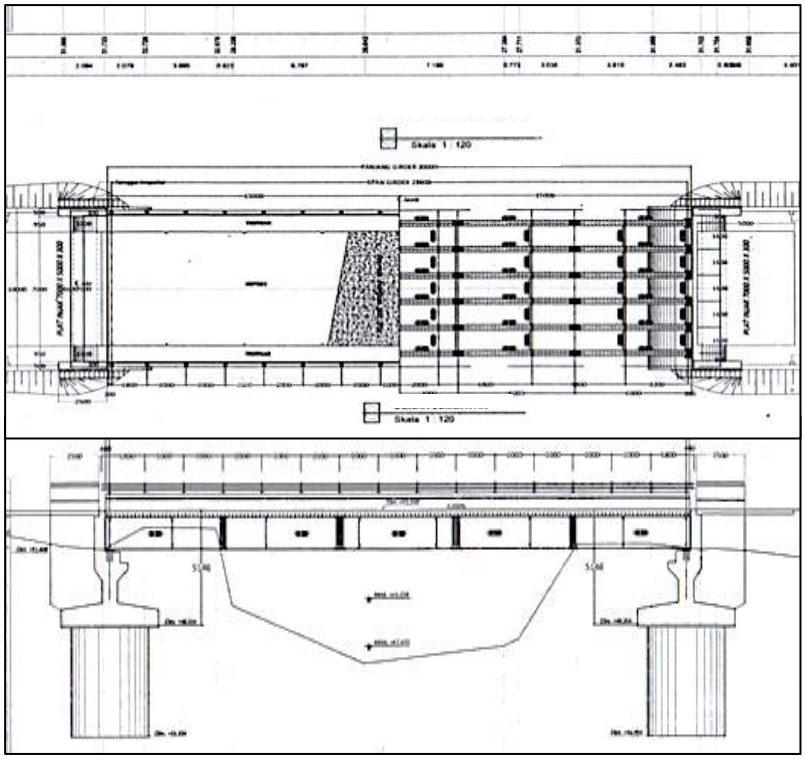

Figure 2. Layout and Long Section of Aifa Bridge

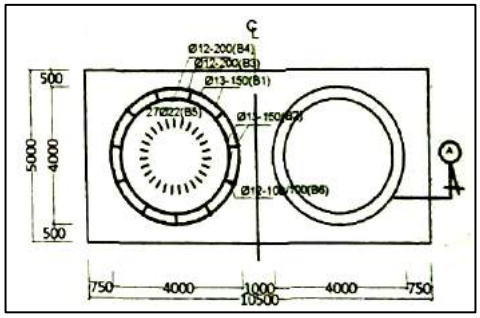

Figure 3. Cross Section of Bridge Foundation

3.2 Results of Soil Investigation

a) Soil Investigation at Point 1

From the results of soil testing conducted in the Soil Testing Laboratory, Department of Civil Engineering, Polytechnic State of Fakfak at the Aifa bridge construction site at Point 1 can be seen in the Table 1. While for the Cone Penetration Test (CPT) conducted, the test results are obtained in Table 2.

Tabel 1. Recapitulation of the Results of Soil Characteristics Test Point 1

No.	Type of Testing	Unit	Test Result
1.	Water content (*w*)	%	17,72
2.	Spesific gravity (G*s*)	-	2,98
3.	Volume of weight (γ)	gr/cm^3	1,096
4.	Atterberg limiy		
	Liquid limit (*LL*)	%	16,75
	Plastic limit (*PL*)	%	NP
	Plasticity index (*PI*)	%	NP
5.	Soil grain analysis		
	Coarse grained soil	%	55,492
	Fine grained soil	%	44,508
6.	Soil classification		
	AASHTO method		A-3
	Unified method		SW-SP
7.	Compaction		
	Optimum water content (W_{opt})	%	33,79
	Volume weight dry (γ_{dry})	gr/cm^3	1,10
8.	Direct shear		
	Cohesion (*c*)	kPa	7,13
	Internal friction angle (ϕ)	^{0}	19,60

Tabel 2. Cone Penetration Test (CPT) Results at Point 1

Depth	Cone Resistance (q_c)	Cone Resistance Total	Swipe Resistance	Sticking Barriers	Value f_s Every 20 cm	Sticking Barriers Total (JHP)	Local Barriers
	q_c	$q_c + f$	f	f_s	F_d	T_f	$F_r = f_s / q_c$
(m)	(kg/cm^2)	(kg/cm^2)	(kg/cm^2)	(kg/cm^2)	(kg/cm)	(kg/cm)	(%)
(1)	**(2)**	**(3)**	**(4)**	**(5)**	**(6)**	**(7)**	**(8)**
0.0	0	0	0	0.0	0	0	0.00
0.2	5	6	1	0.1	2	2	2.00
0.4	10	12	2	0.2	4	6	2.00
0.6	12	15	3	0.3	6	12	2.50
0.8	20	25	5	0.5	10	22	2.50
1.0	18	23	5	0.5	10	32	2.78
1.2	30	39	9	0.9	18	50	3.00
1.4	20	26	6	0.6	12	62	3.00
1.6	80	105	25	2.5	50	112	3.13
1.8	70	92	22	2.2	44	156	3.14
2.0	140	185	45	4.5	90	246	3.21
2.2	200	265	65	6.5	130	376	3.25
2.4	225	300	75	7.5	150	526	3.33
2.6	120	160	40	4.0	80	606	3.33
2.8	43	58	15	1.5	30	636	3.49
3.0	49	67	18	1.8	36	672	3.67
3.2	45	62	17	1.7	34	706	3.78
3.4	40	56	16	1.6	32	738	4.00
3.6	55	78	23	2.3	46	784	4.18
3.8	86	123	37	3.7	74	858	4.30
4.0	100	145	45	4.5	90	948	4.50
4.2	145	215	70	7.0	140	1088	4.83
4.4	300	410	110	11.0	220	1308	3.67

b) Soil Investigation at Point 2

From the results of soil testing conducted in the Soil Testing Laboratory, Department of Civil Engineering, Polytechnic State of Fakfak at the Aifa bridge construction site at Point 2 can be seen in the Table 3. While for the Cone Penetration Test (CPT) conducted, the test results are obtained in Table 4.

Tabel 3. Recapitulation of the Results of Soil Characteristics Test Point 2

No.	Type of Testing	Unit	Test Result
1.	Water content (*w*)	%	17,72
2.	Spesific gravity (G*s*)	-	2,73
3.	Volume of weight (γ)	gr/cm^3	1,026
4.	Atterberg limiy		
	Liquid limit (*LL*)	%	15,485
	Plastic limit (*PL*)	%	NP
	Plasticity index (*PI*)	%	NP
5.	Soil grain analysis		
	Coarse grained soil	%	56,282
	Fine grained soil	%	43,728
6.	Soil classification		
	AASHTO method		A-3
	Unified method		SW-SP
7.	Compaction		
	Optimum water content (W_{opt})	%	33,79
	Volume weight dry (γ_{dry})	gr/cm^3	1,10
8.	Direct shear		
	Cohesion (*c*)	kPa	7,13
	Internal friction angle (ϕ)	^{0}	19,60

Tabel 4. Cone Penetration Test (CPT) Results at Point 2

Depth	Cone Resistance (q_c)	Cone Resistance Total	Swipe Resistance	Sticking Barriers	Value f_s Every 20 cm	Sticking Barriers Total (JHP)	Local Barriers
	q_c	$q_c + f$	f	f_s	F_d	T_f	$F_r = f_s / q_c$
(m)	(kg/cm^2)	(kg/cm^2)	(kg/cm^2)	(kg/cm^2)	(kg/cm)	(kg/cm)	(%)
(1)	**(2)**	**(3)**	**(4)**	**(5)**	**(6)**	**(7)**	**(8)**
0.0	0	0	0	0.0	0	0	0.00
0.2	5	6	1	0.1	2	2	2.00
0.4	10	12	2	0.2	4	6	2.00
0.6	10	12	2	0.2	4	10	2.00
0.8	15	19	4	0.4	8	18	2.67
1.0	20	26	6	0.6	12	30	3.00
1.2	28	37	9	0.9	18	48	3.21
1.4	25	33	8	0.8	16	64	3.20
1.6	50	67	17	1.7	34	98	3.40
1.8	70	96	26	2.6	52	150	3.71
2.0	100	138	38	3.8	76	226	3.80
2.2	120	167	47	4.7	94	320	3.92
2.4	150	210	60	6.0	120	440	4.00
2.6	90	127	37	3.7	74	514	4.11
2.8	40	57	17	1.7	34	548	4.25
3.0	48	70	22	2.2	44	592	4.58
3.2	48	71	23	2.3	46	638	4.79
3.4	50	74	24	2.4	48	686	4.80
3.6	57	85	28	2.8	56	742	4.91
3.8	65	100	35	3.5	70	812	5.38
4.0	80	125	45	4.5	90	902	5.63
4.2	120	189	69	6.9	138	1040	5.75
4.4	135	220	85	8.5	170	1210	6.30
4.6	145	240	95	9.5	190	1400	6.55
4.8	340	420	80	8.0	160	1560	2.35

3.3 Bearing Capacity of The Foundation Using CPT Data

a) Bridge foundation at point 1

The foundation data at point 1 was obtained from Figure 3 cross-sectional of the Aifa bridge foundation with the following data:

- Foundation diameter (D_f) = 400 cm = 4,0 m
- Foundation depth (B) = 400 cm = 4,0 m
- Foundation material = reinforced concrete

Calculation of the bearing capacity of the caison foundation using field test data in Cone Penetration Test results is carried out with the following stages:

1) Calculate N_{SPT} value = q_c / 4 of conversions for each soil layer. For details on determining value N_{SPT} can be seen Table 5.

Tabel 5. Relationship Between the Value of q_c and N correction value

Depth (m)	Cone Resistance (q_c) (kg/cm^2)	N_{SPT} Correction Value	Type of Soil
(1)	**(2)**	**(3)**	**(4)**
0.0	0	0,00	Silt Sand
0.2	5	1,25	Silt Sand
0.4	10	2,50	Silt Sand
0.6	12	3,00	Silt Sand
0.8	20	5,00	Silt Sand
1.0	18	4,50	Silt Sand
1.2	30	7,50	Silt Sand
1.4	20	5,00	Sand
1.6	80	20,00	Sand
1.8	70	17,50	Sand
2.0	140	35,00	Sand
2.2	200	50,00	Sand
2.4	225	56,25	Sand
2.6	120	30,00	Sand
2.8	43	10,75	Sand
3.0	49	12,25	Sand
3.2	45	11,25	Sand
3.4	40	10,00	Sand
3.6	55	13,75	Sand
3.8	86	21,50	Sand
4.0	100	25,00	Sand
		$\sum$ = 342	

2) Calculate end bearing capacity foundation (Q_p)

A_p = ¼ x π x (D^2) (1)
= 0,25 x 3,14 x (4^2)
= 12,56 m^2

Q_p = 40 x N_p x A_p (2)
= 40 x 25,00 x 12,56
= 12.560,00 kN

3) Calculate friction skin foundation (Q_s)

A_s = π x D x t (3)
= 3,14 x 4,0 x 4,0
= 50,24 m^2

$N_{average}$ = $\sum N_{SPT}$ / n (4)
= 342 / 20
= 17,10

Q_s = 0,1 x N x A_s (5)
= 0,1 x 17,10 x 50,24
= 85,91 kN

4) Calculate self weight of foundation (W_p)

W_p = [(¼.π.($D_{outside}^2$-D_{inside}^2) x D_f x bj. concrete] + [(1/4.π.D_{inside}^2) x Df x bj. cyclop] (6)
= [(¼ x 3,14 x (4^2-$3{,}70^2$) x 4,00 x 24,00] + [¼ x 3,14 x ($3{,}70^2$) x 4 x 22,00]
= (174,082) + (945,705)
= 1.119,787 kN

5) Calculate ultimate bearing capacity foundation (Q_{ult})

Q_{ult} = $Q_p + Q_s - W_p$ (7)
= 12.560,00 + 85,91 – 1.119,787
= 11.522,54 kN

6) Calculate allowable bearing capacity foundation (Q_{all})

Q_{all} = Q_{ult} / FS (8)
= 11.526,12 / 2,5
= 4.610,44 kN

b) Bridge foundation at point 2

The foundation data at point 1 was obtained from Figure 3 cross-sectional of the Aifa bridge foundation with the following data:

- Foundation diameter = 400 cm = 4,0 m
- Foundation depth = 400 cm = 4,0 m
- Foundation material = reinforced concrete

Calculation of the bearing capacity of the caison foundation using field test data in Cone Penetration Test results is carried out with the following stages:

1) Calculate N_{SPT} value = q_c / 4 of conversions for each soil layer. For details on determining value N_{SPT} can be seen Table 6.

Tabel 6. Relationship Between the Value of q_c and N_{SPT} Correction Value

Depth (m) (1)	Cone Resistance (q_c) (kg/cm^2) (2)	N_{SPT} Correction Value (3)	Type of Soil (4)
0.0	0	0,00	Silt Sand
0.2	5	1,25	Silt Sand
0.4	10	2,50	Silt Sand
0.6	10	2,50	Silt Sand
0.8	15	3,75	Silt Sand
1.0	20	5,00	Silt Sand
1.2	28	7,00	Silt Sand
1.4	25	6,25	Silt Sand
1.6	50	12,50	Silt Sand
1.8	70	17,50	Silt Sand
2.0	100	25,00	Silt Sand
2.2	120	30,00	Silt Sand
2.4	150	37,50	Silt Sand
2.6	90	22,50	Sand
2.8	40	10,00	Sand
3.0	48	12,00	Sand
3.2	48	12,00	Sand
3.4	50	12,50	Sand
3.6	57	14,25	Sand
3.8	65	16,25	Sand
4.0	80	20,00	Sand
		∑ = 270,25	

2) Calculate end bearing capacity foundation (Q_p)

A_p = ¼ x π x (D^2) (1)
= 0,25 x 3,14 x (4^2)
= 0,25 x 3,14 x (4^2)
= 12,56 m^2

Q_p = 40 x N_p x A_p (2)
= 40 x 20,00 x 12,56
= 10.048,00 kN

3) Calculate friction skin foundation (Q_s)

A_s = π x D x t (3)
= 3,14 x 4,0 x 4,0
= 50,24 m^2

$N_{average}$ = ∑ N_{SPT} / n (4)
= 270,25 / 20
= 13,51

Q_s = 0,1 x N x A_s (5)
= 0,1 x 13,51 x 50,24
= 67,87 kN

4) Calculate self weight of foundation (W_p)

W_p = [(¼.π.($D_{outside}^2$-D_{inside}^2) x D_f x bj. concrete] + [(1/4.π.D_{inside}^2) x Df x bj. cyclop] (6)
= [(¼ x 3,14 x (4^2-$3,70^2$) x 4,00 x 24,00] + [¼ x 3,14 x ($3,70^2$) x 4 x 22,00]
= (174,082) + (945,705)
= 1.119,787 kN

5) Calculate ultimate bearing capacity foundation (Q_{ult})

Q_{ult} = Q_p + Q_s - W_p (7)
= 10.048,00 + 67,87 – 1.119,787
= 8.996,10 kN

6) Calculate allowable bearing capacity foundation (Q_{all})

Q_{all} = Q_{ult} / FS (8)
= 8.996,10 / 2,5
= 3.598,43 kN

3.4 Bearing Capacity of Foundation Using Soil Parameter Data

a) Bridge foundation at point 1

The foundation data at point 1 was obtained from Figure 3 cross-sectional of the Aifa bridge foundation with the following data:

- Foundation diameter (B) = 400 cm = 4,0 m
- Foundation depth (D_f) = 400 cm = 4,0 m
- Volume of weight (γ) = 1,096 gr/cm^3 x 9,81 = 10,75 kN/m^3
- Cohesion (*c*) = 7,133 kPa = 7,133 kN/m^2
- Internal friction angle (ϕ) = $19,60^0$

Calculation of the bearing capacity of the caison foundation using soil parameter data results is carried out with the following stages:

1) Determine the bearing capacity factor of the foundation, (N_c, N_q, N_γ)
From the table of Terzaghi's bearing capacity factor values:
N_c = 17,316 ; N_q = 7,160 dan N_γ = 4,696

2) Calculate end bearing capacity foundation (Q_p)

A_p = ¼ x π x (D^2) (1)
= 0,25 x 3,14 x ($4,0^2$)
= 12,56 m^2

q_u = 1,3.c.N_c + D_f.γ.N_q + 0,3.ɤ.B.N_γ (9)
= (1,3 x 7,133 x17,316) + (4 x 10,75 x 7,160) + (0,3 x 10,75 x 4,0 x 4,696)
= (160,57) + (307,88) + (60,58)
= 529,03 kN

Q_p = q_u x A_p (10)
= 529,03 x 12,56
= 6.644,62 kN

3) Calculate self weight of foundation (W_p)

W_p = [(¼.π.($D_{outside}^2$-D_{inside}^2) x D_f x bj. concrete] + [(1/4.π.D_{inside}^2) x Df x bj. cyclop] (6)
= [(¼ x 3,14 x (4^2-$3,70^2$) x 4,00 x 24,00] + [¼ x 3,14 x ($3,70^2$) x 4 x 22,00]
= (174,082) + (945,705)
= 1.119,787 kN

4) Calculate ultimate bearing capacity foundation (Q_{ult})

Q_{ult} = Q_p + Q_s - W_p (7)

= 6.644,62 + 0 - 1.119,787
= 5.524,83 kN

5) Calculate allowable bearing capacity foundation (Q_{all})

Q_{all} = Q_{ult} / FS (8)
= 5.524,83 / 2,5
= 2.209,93 kN

b) Bridge foundation at point 2

The foundation data at point 2 was obtained from Figure 3 cross-sectional of the Aifa bridge foundation with the following data:

- Foundation diameter (B) = 400 cm = 4,0 m
- Foundation depth (D_f) = 400 cm = 4,0 m
- Volume of weight (γ) = 1,096 gr/cm^3 x 9,81 = 10,65 kN/m^3
- Cohesion (c) = 16,030 kPa = 16,030 kN/m^2
- Internal friction angle (ϕ) = 4,46%

Calculation of the bearing capacity of the caison foundation using soil parameter data results is carried out with the following stages:

1) Determine the bearing capacity factor of the foundation, (N_c, N_q, N_γ)
From the table of Terzaghi's bearing capacity factor values:
N_c = 7,127 ; N_q = 1,535 dan N_γ = 0,446

2) Calculate end bearing capacity foundation (Q_p)

A_p = ¼ x π x (D^2) (1)
= 0,25 x 3,14 x (4,0^2)
= 12,56 m^2

q_u = 1,3.c.N_c + D_f.γ.N_q + 0,3.ɤ.B.N_γ (9)
= (1,3 x 16,030 x 7,127) + (4 x 10,65 x 1,535) + (0,3 x 10,65 x 4,0 x 0,446)
= (148,52) + (65,39) + (5,70)
= 219,61 kN

Q_p = q_u x A_p (10)
= 219,61 x 12,56
= 2.758,31 kN

3) Calculate self weight of foundation (W_p)

W_p = [(¼.π.($D_{outside}^2$-D_{inside}^2) x D_f x bj. concrete] + [(1/4.π.D_{inside}^2) x Df x bj. cyclop] (6)
= [(¼ x 3,14 x (4^2-3,70^2) x 4,00 x 24,00] + [¼ x 3,14 x (3,70^2) x 4 x 22,00]
= (174,082) + (945,705)
= 1.119,787 kN

4) Calculate ultimate bearing capacity foundation (Q_{ult})

Q_{ult} = Q_p + Q_s - W_p (7)
= 2.758,31 + 0 - 1.119,787
= 1638,52 kN

5) Calculate allowable bearing capacity foundation (Q_{all})

Q_{all} = Q_{ult} / FS (8)
= 1638,52 / 2,5
= 655,41 kN

4. CONCLUSION

Based on the results of research and data analysis that has been carried out, the following conclusions can be drawn:

1. From the results of testing the soil characteristics in the laboratory, the type of soil at point 1 is the type of good to bad graded sand soil (SW-SP) with a water content of 17.72%, specific gravity 2.98, liquid limit (LL) = 16,746% included in the non-plastic category. While the location of point 2 is obtained from good to bad graded sand soil type (SW-SP) with a water content of 28.52%, specific gravity 2.73, liquid limit (LL) = 16.746% including the non-plastic category.
2. From the analysis of the calculation of the bearing capacity of the foundation Aifa bridge using data from the sondir test results for point 1 was obtained allowable bearing capacity (Q_{all}) is 4.610,44 kN and for point 2 was obtained allowable bearing capacity (Q_{all}) is 3.598,43 kN. For calculating bearing capacity of the foundation using soil parameter data for point 1 was obtained bearing capacity allowable (Q_{all}) is 2.209,93 kN and for point 2 was obtained allowable bearing capacity (Q_{all}) is 655,41 kN.

5. ACKNOWLEDGEMENT

The authors wish to acknowledge the Ministry of Research, Technology and Higher Education Republic of Indonesia (RISTEKDIKTI-RI) for providing the funds for this research with scheme Beginner Lecturer Research (PDP) year 2019. The author also thanks Ministry of Public Works of the Directorate General of Highways (BPJN XVII Manokwari) for technical data and detail engineering design Aifa bridge.

6. REFERENCES

[1] AASHTO. 1997. Bridge Management System. Jakarta: Departemen Pekerjaan Umum
[2] Anonymous. 1986. Peraturan Pembebanan Jembatan Jalan Raya. Jakarta: Departemen Pekerjaaan Umum
[3] Balamba, S., Sompie, O.B.A., Sarajar, A. 2013. Analisis Kestabilan Pondasi Jembatan Studi Kasus: Jembatan Essang Lalue. Jurnal Sipil Statik Volume 1 Nomor 11
[4] Bowles, J.E., (1996), *Foundation Anaysis and Design*, McGraw-Hill, New York
[5] Budi, G.S. 2011. Pengujian Tanah di Laboratorium. Surabaya: Graha Ilmu
[6] Das, Braja, M. 2007. Principles of Foundation Engineering 7th Edition. Standford: Global Engineering
[7] Hardiyatmo, H.C. 2011. Analisis dan Perancangan Pondasi 1. Yogyakarta: Gadjah Mada University Press,
[8] Murthy, V.N.S. 2007. Advanced of Foundation Engineering. New Delhi Balgalore: CBS
[9] Supriadi, B., Muntohar, A.S. 2007. Jembatan. Yogyakarta: Beta Offset
[10] SNI 2827-2008. 2008. Cara Uji Penetrasi Lapangan dengan Alat Sondir. Jakarta: Badan Standardisasi Nasional
[11] Yunus, M. 2015. Panduan Praktikum Laboratorium Uji Tanah. Jurusan Teknik Sipil: Politeknik Negeri Fakfak

LOGIC
Journal of Engineering Design and Technology
Vol. 19 No.3 November 2019; p. 155 - 161

p-ISSN : 1412-114X
e-ISSN : 2580-5649
http://ojs.pnb.ac.id/index.php/LOGIC

EFFECT OF UV AGING ON PHYSICAL PROPERTIES OF VULCANIZED RUBBER WITH THE ADDITION OF RECLAIMED RUBBER

Muh Wahyu Syabani [1)], Yuli Suwarno [2)], Mertza Fitra Agustian [3)]

1,2,3) Department of Rubber and Plastic Processing Technology, Politeknik ATK Yogyakarta, Jl Ring Road Selatan, Panggungharjo, Sewon, Bantul, DI Yogyakarta

Correponding email [1)] : mw-syabani@kemenperin.go.id

Abstract. Rubber solid waste amount increased continuosly and caused environmental problem since it is very difficult to be naturally degraded. Therefore, the interest of using rubber waste as raw material for new rubber product is increased. Reclaimed rubber can be used as filler aditif for rubber processing. The aim of this research was to study the effect of UV aging on the rubber product as the reclaimed filler added. The mixing of the rubber and the additives used the kneader and open mill. The vulcanization process was done by hydraulic press. In this research, the reclaimed rubber addition was varied as follows: 12,5; 37,5 and 62,5 phr. The products quality differences before and after the UV aging evaluated using physical tests. The result of FTIR showed that the polymer chain were broken by ultraviolet radiation. The physical test gives result that the hardness and tensile strength decreased, but the elongation is increased after UV aging.

Keywords : UV aging; Rubber waste; Reclaimed rubber; Physical properties; Environmental.

1. INTRODUCTION

Rubber are important elastomer [1], but since vulcanized rubbers having crosslinked structure and contain many additive its cannot degradated easily [2][3]. The solid waste potentially damaged the environment if dumped without proper treatment [4]. Many attempt has been made to solved the problems, such as landfill, electrical generator and pirolysis [2][5][6]. But, there are still many problems faced from the system, thus its needed alternative methods for rubber solid waste managements [7].

Solid waste of rubber could be used as filler to subsitute some of the rubber raw materials in compound processing [8]. This subsitution can reducing the amount of rubber solid waste significantly, lowering the production cost, and also improving the product characteristic such as the uniformity and dimension stability [2][8][9]. In our previous works, higher amount reclaimed rubber addition could increased hardness of the vulcanized rubber, but also gaves lower abrasion resistance and elongation at break [10].

In recent years, the characterization of vulcanized rubber has been studied in many research, however the testing are usually done for the new products. The application of the product are prone to aging under external environments, such as temperature, ultraviolet radiation and humidity. Materials aging's lead to changes in product characteristic and realibility [11][12]. The evaluation of the aging condition was important factor to analysis the materials stability [13], thus could helps to made better material preferences, predicted the wear reliability and avoided failure application of the product. Meanwhile, although the effect of aging for elastomer structure and characteristic change got many attention from researcher [14], but the effect of ultraviolet radiation to elastomer had not been established yet [15][16]. Its well known that ultraviolets radiation as part of sun rays could break the polymer chain of the materials. Eventhough, Rasool [3] reported different result which the addition of reclaimed rubber gave better aging resistance.

The aims of this research were to studying the effect of ultraviolet radiation on the vulcanized rubber. Reclaimed rubber from solid waste were used as filler for the rubber processing. The samples were conditioned on the ultraviolet chamber at certained times then analyzed using FTIR and physical testing. The results could

gave deeper understanding on vulcanized rubbers aging condition, thus could be used as guide to choose appropriate materials and predicted the wearing age.

2. METHODS

Material

The rubber compound were consisted of brown crepe and compo crepe as raw materials. The filler that be used were reclaimed rubber, silica and carbon black. Minarex oil were used as plasticizer, glycolipoprotein extract (G-90) and trimethyl dihydroquinoline polymer (TMQ) as antioxidant and antidegradation. Zinc oxide (ZnO) and stearic acid as an activator. Tetra methyl thiuram monosulfide (TMTM) and n-cyclohexyl-2-benzothiazole sulfenamide (CBS) as an accelerator, and sulfur as a vulcanizing agent.

Research Equipment

The tools that used in this experiment consisted of kneader and open mill for compounding process and the hydraulic hot press for vulcanization process. Rubber hardness were measured using Durometer (Shore A). Universal testing machine (Gester GT K-02) were used to measure the tensile strength and elongation at break. The functional groups of materials surface were confirmed using FT-IR (Perkin-Frontier). The aging process simulation was using Ultraviolet-Tester (Atlas UV Test II).

Research Variable

The study of this research were focused on the addition factor of reclaimed rubber and aging time. The variation amount of reclaimed rubber were 12.5, 37.5, and 62.5 phr. Aging time variation were conducted by time span 0, 72, and 120 hours respectively.

Method

Raw materials were masticated using kneader. The masticated material was then mixed with activator, antioxidant and antidegradation, filler, and plasticizer consecutively until homogenous. The process was followed by mixing accelerators and vulcanization agents using open mill machines. Maximum temperature during compounding process was 70^{o}C. The cooled compound sheet (±37^{o}C) was then vulcanized using a hydraulic hot press at temperature of 160^{o}C and a pressure of 100 kg/cm^2 for 15 minutes. Vulcanized rubber was then ready for testing.

Testing

Vulcanized rubber with a thickness of 2±0.2 mm was cut to the size of each test sample, then placed on a holder and mounted in a UV tester. The test sample was made with three replications. The beam of ultraviolet radiation that used has a wavelength range of 280 to 315 nm. The distance between the sample and the source of the lamp was set uniformly. The temperature used was 32^{o}C according to the average temperature of the environment in the tropics. Aging time variation were conducted by time span 0;72; and 120 hours. Functional group transformation of the sample were analyzed using FTIR. While the physical properties were tested according to SNI 0778: 2009 and ISO 37: 2011 which included the values of hardness, tensile strength and elongation at break.

3. RESULTS AND DISCUSSION

3.1. FTIR Analysis

The effect of ultraviolet radiation were the function of penetration depth and radiation times [15]. Thus, to avoid the penetration depth variation, then the distances of the samples to ultraviolet lamp were setted using same arrangement for all samples. After aging simulation for 120 hours, visually there is no difference for all the samples. But, when the surface of the sample were rubbed, the sample with 120 hours aging had more oily texture than the 72 hours sample. The same condition also occured for all the three reclaimed rubber addition variation.

When the ultraviolet radiation got in and adsorbed by the vulcanized rubber, the homogenous materials compound could change its behaviors [15]. The solubility of the additives in compound might be reduced and blooming to the surface. The identification of the loss of additives done by using the FTIR analysis. Fig 1, 2 and 3 below showed that the FTIR spectra of the vulcanized rubber with aging time for the addition of reclaimed rubber 12.5, 37.5 and 62.5 phr respectively. There are three functional groups wavelength that chracterize the change which are 2900, 2112 and 1365 cm^{-1}. According to Liu [13], the number identified as aliphatic chain of C-H, accelerator excess of –N=C=S, and antioxidant C-N.

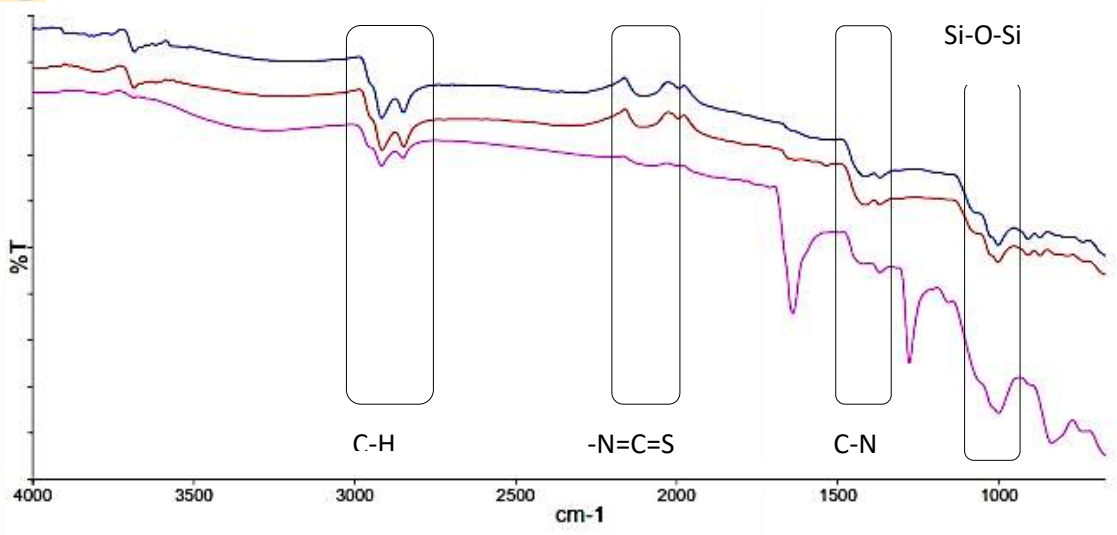

Figure 1. FTIR analysis for 12.5 phr reclaimed rubber

Absorbance measurements using FTIR for 12.5 phr were showed in Fig. 1. Its showed that all of three characterizing functional groups were relatively similar with the aging time variation. Thus, the amount of the additives in the each samples didnt change. There is only difference in the 1365 cm-1 spectra that gave slightly lower peak that indicates the decreased of the antioxidant amount. Antioxidant had function to reduce the materials defect from the aging. From the figure, we also showed that there isi decreased peak in 1000 cm-1 spectra that indicated the break of the Si-O-Si chain of the elastomer.

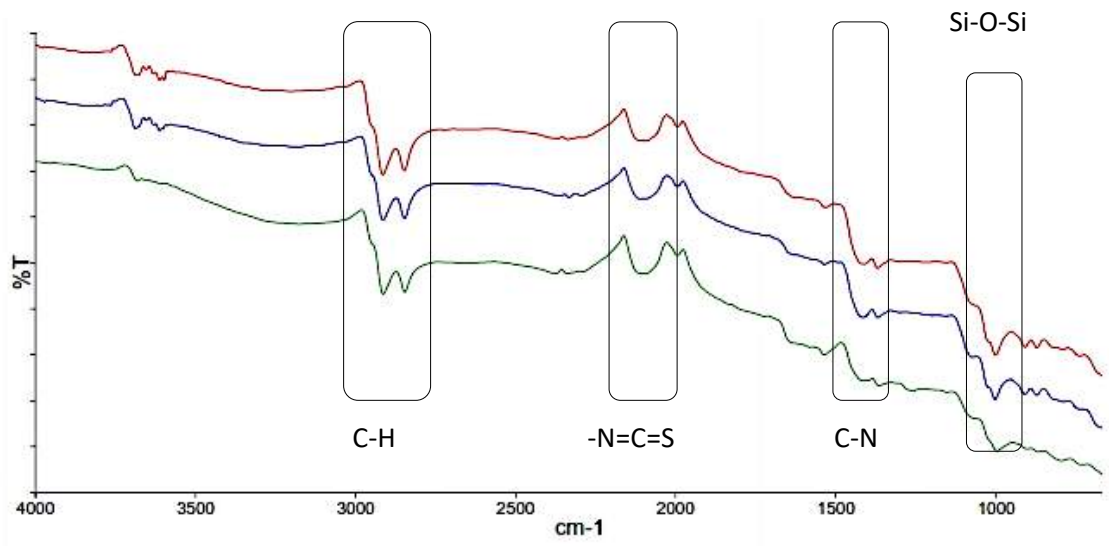

Figure 2. FTIR analysis for 37.5 phr reclaimed rubber

Fig. 2 showed that the adsorbance measurement for the addition of 37.5 phr reclaimed rubber in to vulcanized rubber. Similar trends were also occured, three characterizing functional groups only gave slight differences. Thus, we could made conclusion that the loss of the additives were very slow for the aging time.

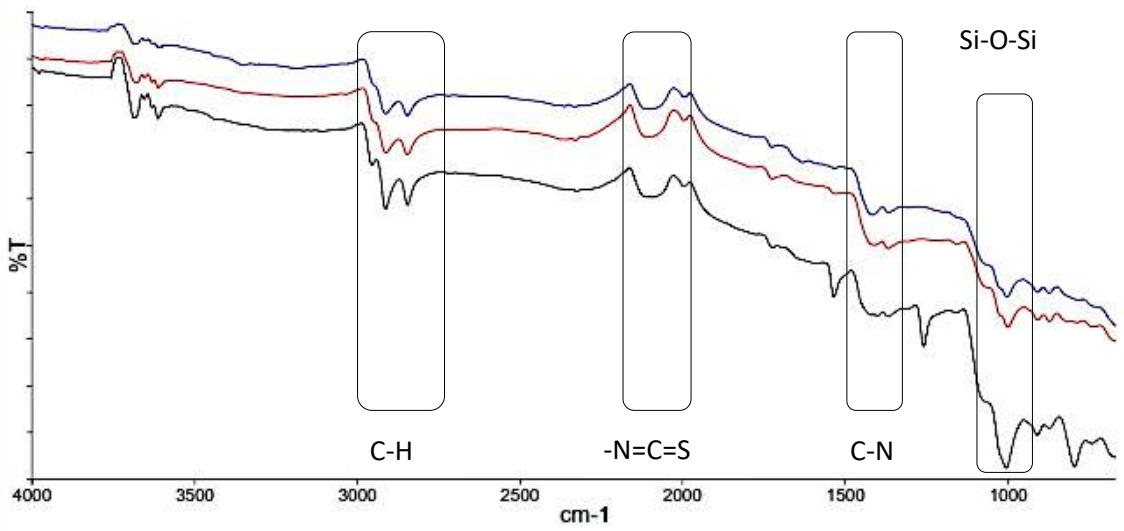

Figure 3. FTIR analysis for 62,5 phr reclaimed rubber

Similar result also presented for the addition of 62.5 phr reclaimed rubber as showed in fig. 3. Therefore, on these samples, the occurence of the additives were also could be maintained. But, some of the additives solubility decreased then blooming to the vulcanized rubber surface. Nevertheless, at the vibration spectra of 1000 cm-1 showed lower absorbance that indicating the braking of the Si-O-Si chain.

Effects of Aging on Tensile Strength of Vulcanized Rubber

Tensile strength is a measurement of the force required to pull vulcanized rubber to the point where it breaks. Reclaimed rubber is solid rubber waste that has undergone vulcanization so that it is more difficult to form new bonds [10], while weak interactions between elastomers and fillers will have an impact on the mechanical characteristics of vulcanization [7] one of which is decreasing of tensile strength value [17]. Figure 4 below shows the effect of aging time for each sample with variations of reclaimed rubber addition.

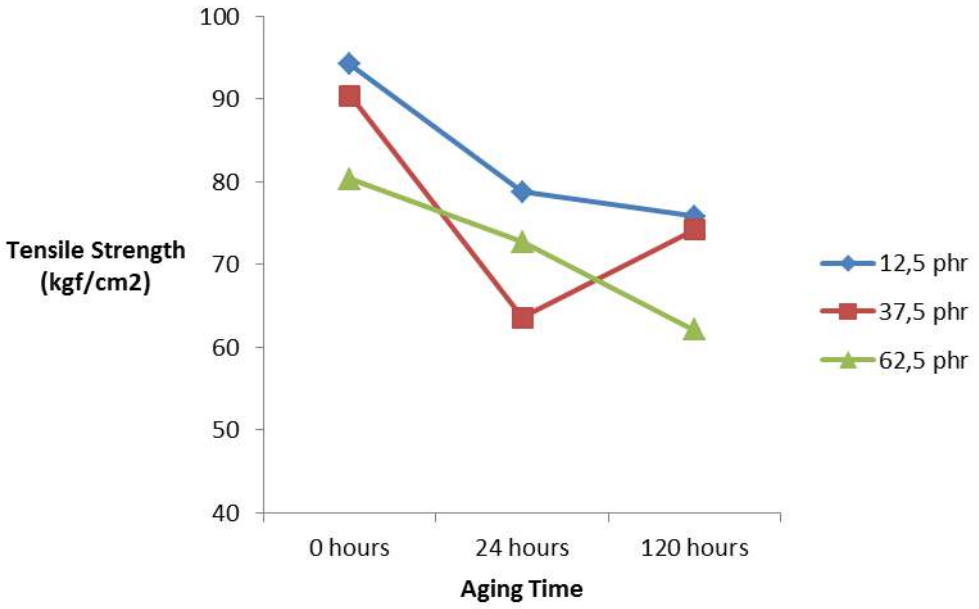

Figure 4. Tensile Strength Test Results
Source: Primary data processed, 2018

During aging, all three vulcanized rubber samples have similar tendency, that is the tensile strength value decreased with the longer aging time. The polymer chain will absorb radiation and when its value is higher than ionization energy it will cause radical formation [15]. The more radiation received will cause the polymer bonds to be damaged, so that the value of vulcanized rubber strength will also decrease. This is because the bond formation between the reclaimed rubber chain and the new rubber is more difficult than the new rubber polymer

chains. The bond between filler and elastomer is also weaker [10] making it easier to break when exposed to ultraviolet radiation. This tendency is clould be clearly seen in Figure 4, where more addition of reclaimed rubber will result in decreasing of tensile strength faster along the aging treatment.

Effects Of Aging On Elongation Break

The elongation at break shows the ability of vulcanized rubber to stretch when pulled until it breaks. Its value is useful for determining the selection of materials suitable for applications that require elasticity such as belts, seals, outsoles and others. In our previous study, the elasticity of vulcanization will decrease in line with the increasing number of reclaimed rubber [10]. This is because the reclaimed rubber has vulcanized so that it carries a cross bond. The existence of this cross bond will reduce the freedom of movement between polymer molecules. The test results for the breakout elongation are shown in Figure 5.

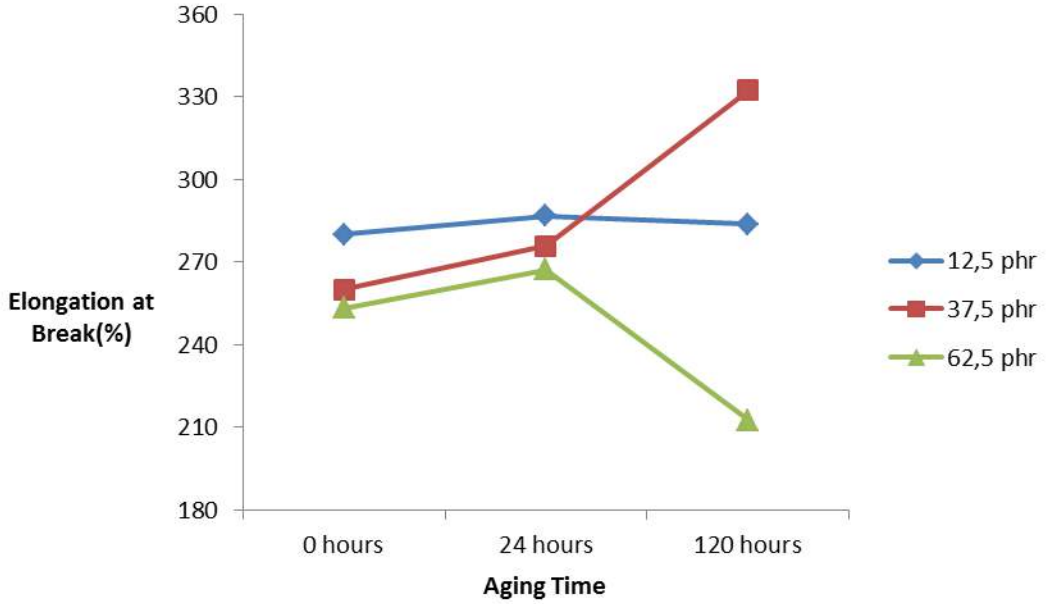

Figure 5. Elongation at Break Test Results
Source: Primary data processed, 2018

Aging causes a breakdown of some bonds between polymer chains [14], allowing slip movement between molecules. The ease of this movement can be seen from the increased vulcanized rubber elasticity. Seen in Figure 5, each sample has the same tendency, that is, elongation at break will increase at 72 hours aging time. Similar research conducted by Wu [12] also give harmonious results. Aging causes the net structure of elastomers to be damaged [11]. The elongation at break value has increased in aging 120 hours which shows that the number of broken bonds is increasing. However, it is interesting to see that the addition of reclaimed rubber 62.5 phr has the lowest increase of elongation at break. It can be explained that recycled rubber already carries a cross bond so that it has a greater crosslink density for vulcanized rubber with the addition of more reclaimed rubber.

The elasticity of vulcanized rubber is also influenced by plasticizers, where the value will decrease if the amount of plasticizer is also reduced [13]. Aging due to the influence of temperature has the potential to cause evaporation of plasticizers [13], but in this study it was seen that aging due to the influence of ultraviolet light did not have the same tendency. FTIR results indicate the presence of additives can be maintained, so that the elongation at break value is more influenced by the presence of crosslinking.

Effects of Aging on the Level Hardness

Hardness affects the appearance and durability of rubber products, and its value is related to the amount of filler added [4]. The more reclaimed rubber is added will provide a higher value of hardness [10]. This is due to the increase in the value of crosslink density from vulcanized rubber [7] as a result of cross-link formation between elastomers and reclaimed rubber. The results of the hardness test are presented in Figure 6 below.

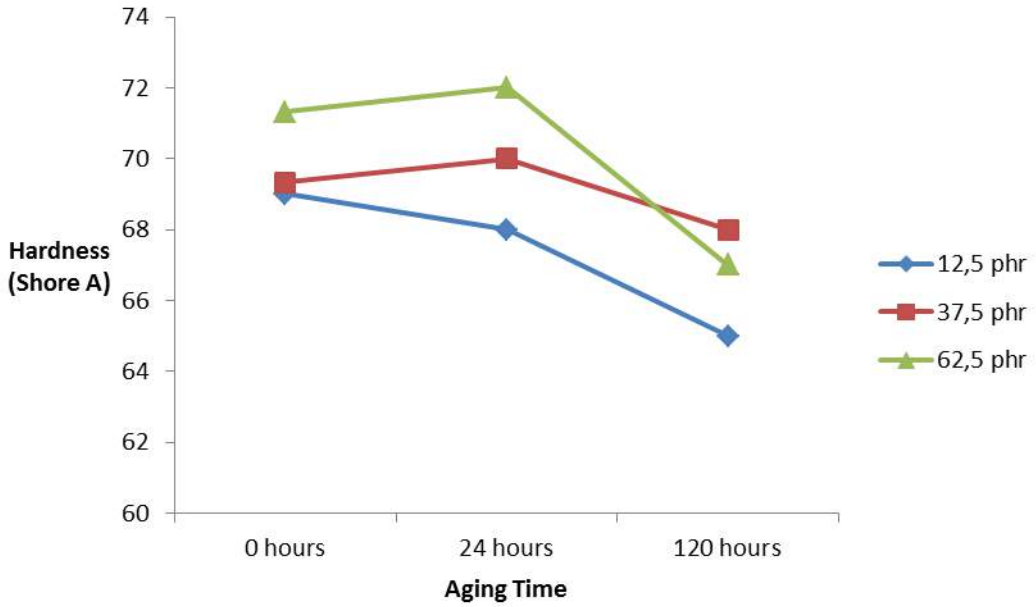

Figure 6. Hardness Test Results
Source: Primary data processed, 2018

At 72 hours aging, it can be seen in figure 7 that the hardness value will tend to increase except for vulcanized rubber with the addition of 12.5 phr. According to Goga [15] the main influence of the aging process is increasing crosslink density on the surface of the sample. Increasing cross-link density will cause the material to become hard [12]. When exposed to ultraviolet light, the surface of the sample will receive the most radiation, and the radiation value will decrease with increasing penetration depth. This causes the surface of the sample conditions are relatively different from the inside, while the hardness test is carried out on the surface of the sample. However, in aging 120 hours, more ultraviolet light radiation is received by the sample, and the more the bonds between the polymer rubber chains are broken. This is inline with the FTIR results which show the breakdown of Si-O-Si bonds in elastomers. The decrease in crosslink density causes a decrease in the hardness value of vulcanized rubber. At higher values, it will produce cracks and holes on the vulcanized rubber surface [12][16].

4. CONCLUSION

In this study, UV aging of the vulcanized rubber with the addition of the reclaimed rubber as a filler were studied using FTIR and physical testing. FTIR spectra shows that the during aging the additive were stay in the vulcanized rubber, but its solubility were decreased. UV aging effected the characteristic of the vulcanized rubber that it improve the formation of polymer network of the unsaturated vulcanized. Higher crosslink density of the vulcanized will improve the hardness, but for over 72 hours of aging will made trhe crosslink bond deteriorated, thus decreased the tensile strength and hardness. Futhermore, the breaking of the bond will make the polymer easily to moves, thus gives higher elongation at break. For better undestanding of the aging effect on the vulcanized, it need further research on the thermal and humidity aging simulation that close to real environmental aging.

5. ACKNOWLEDGEMENT

The authors gratefully acknowledge use of the services and facilities at the Politeknik ATK Yogyakarta, especially at the Workshop of Rubber Processing and Laboratory of Instrumentation.

6. REFERENCES

[1] C. Li, J. Zhong, L. Yang, S. Li, L. Kong, and T. Hou, “Studies on the Properties and The Thermal Decomposition Kinetics of Natural Rubber Prepared with Calcium Chloride”, *e-Polymers*, vol. 072, pp. 1-9, 2010.

[2] B. Adhikari, D. De, and S. Maiti, “Reclamation and recycling of waste rubber”, *Prog. Polym. Sci*., vol. 25, pp. 909–948, 2000.

[3] R.T. Rasool, S. Wang, Y. Zhang, Y. Li, and G. Zhang, "Improving the aging resistance of SBS modified asphalt with the addition of highly reclaimed rubber". *Contruction and Building Materials*, vol. 145, pp. 126-134, 2017.
[4] A. Yuniari, M. Sholeh, and I.N. Indrajati, "Pengaruh Sistem Vulkanisasi Konvensional (CV) dan Semi Efisien (SEV) terhadap Sifat Aging dan Termal Vulkanisat Campuran Karet Alam dan Karet Butil", *Majalah Kulit Karet dan Plastik.* vol. 31, no. 2, pp. 99-106, 2015.
[5] D.C. Bomberger, and J.L. Jones, "An Evaluation of Modular Incinerators for Energy Recovery From Solid Wastes", *ACS Symposium Series* vol. 130, *Thermal Conversion of Solid Wastes and Biomass Chapter 6*, pp. 67-83, 1980.
[6] K. Shigeo, K. Inoue, H. Tanaka, and T. Sakai, "Pyrolysis Process for Scrap Tires", *ACS Symposium Series* vol. 130, *Thermal Conversion of Solid Wastes and Biomass Chapter 40*, pp. 557-572, 1980.
[7] K. Formela, D. Wasowicz, M. Formela, A. Hejna, and J. Haponiuk, "Curing Characteristics, Mechanical and Thermal Properties of Reclaimed Ground Tire Rubber Cured with Various Vulcanizing Systems", *Iran Polym. J.* vol. 24, no. 4, pp. 289-297, 2015.
[8] P. Setyowati, Pramono, and Supriyanto, "Pemanfaatan Karet Riklim Dari Skrab Rubber Roll Untuk Kompon Sol Sepatu", *Majalah Kulit, Karet dan Plastik*, vol. 22, no. 1, pp. 38-44, 2006.
[9] F.J. Navarro, P. Partal, F. Martinez-Boza, and C. Gallegos, "Influence of Crumb Rubber Concentration on the Rheological Behavior of a Crumb Rubber Modified Bitumen", *Energy Fuels*., vol. 19, pp. 1984-1990, 2005.
[10] M.W. Syabani, F.I. Fauziyyah, and T. Mutiara, "Pengaruh penambahan karet reklim dari limbah outsole terhadap sifat fisis dan sifat thermal produk outsole sepatu (Studi kasus di CV. Carita Niaga)". *Jurnal Sains dan Teknologi Lingkungan*, vol. 10, no. 1, pp. 26-40, 2018.
[11] C. Neuhaus, A. Lion, M. Johlitz, P. Heuler, M. Barkhoff, and F. Duisen, "Fatigue behavior of an elastomer under consideration of ageing effects". *International Journal of Fatigue*, vol. 104, pp. 72-80, 2017.
[12] J. Wu, K. Niu, B. Su, and Y. Wang, "Effect of combined UV thermal and hydrolytic aging on micro-contact properties of silicone elastomer". *Polymer Degradation and Stability*, vol. 151, pp. 126-135, 2018.
[13] X. Liu, J. Zhao, R. Yang, R. Lervolino, and S. Barbera, "A novel in-situ aging evaluation method by FTIR and the application to thermal oxidized nitrile rubber". *Polymer Degradation and Stability*, vol. 128, pp. 99-106, 2016.
[14] Q. Wang, S. Li, X. Wu, S. Wang, and C. Ouyang, "Weathering aging resistance of different rubber modified asphalts". *Contruction and Building Materials*, vol. 106, pp. 443-448, 2016.
[15] N.O. Goga, D.E. Demco, J. Kolz, R. Ferencz, A. Haber, F. Casanova, and B. Blumich, "Surface UV aging of elastomer investigated with microscopic resolution by single-sided NMR", *Journal of Magnetic Resonance*, vol. 192, pp. 1-7, 2008.
[16] Y. Qin, J. Fu, L. Yu, Z. Yang and W. Guo, "Comparative research on aging properties of HTV silicon rubber via outdoor electric aging and ultraviolet accelerated aging". *Advanced Materials Research*, vol. 641-642, pp. 333-337, 2013.
[17] A.M. Ajam, S.H. Al-Nesrawy, and M. Al-Maamori, "Effect of Reclaim Rubber Loading on The Mechanical Properties of SBR Compoisite". *Int. J. Chem. Sci.*, vol. 14, no. 4, pp. 2439-2449, 2016.

LOGIC
Journal of Engineering Design and Technology
Vol. 19 No.3 November 2019; p. 162 - 168

p-ISSN : 1412-114X
e-ISSN : 2580-5649
http://ojs.pnb.ac.id/index.php/LOGIC

FORCE BASED DESIGN AND DIRECT DISPLACEMENT BASED DESIGN FOR DUAL SYSTEM STRUCTURE

Annisaa Dina Puspita D[1)], Anis Rosyidah[2)]

1) Department of Civil Engineering, Politeknik Negeri Jakarta
2) Department of Civil Engineering, Politeknik Negeri Jakarta

Correponding email:
[1)]annisaadina06@gmail.com
[2)]anis.rosyidah@sipil.pnj.ac.id

Abstract. The Force Based Design (FBD) and the Direct Displacement-Based Design (DDBD) are methods for designing seismic-resistant buildings. Building structures designed, are expected to be suitable with the purpose and usefulness of a building. For this reason, this study compares the performance of dual system structures using the DDBD and FBD methods that aim to prove better performance with consideration of safety against users during an earthquake. This research method uses design analysis method to compare the value of the base shear force, reinforcement ratio, and performance level using software for static nonlinear pushover analysis. The results showed the value of the base shear force x direction of the DDBD method was 17.57% smaller than the FBD method, whereas for the y direction the DDBD value was greater than 9.38% of the FBD. The value of the reinforcement ratio of the beam, column and shear wall results is greater DDBD than FBD. The actual drift of the DDBD and FBD methods is slightly different. So that both are at the same level of performance, namely damage control. The performance level has not reached the performance target of life safety design in DDBD, but the structure has met the level performance requirements for offices.

Keywords : Dual System, DDBD, FBD

1. INTRODUCTION

In multi-story building planning, the structure of a building must be able to withstand earthquake forces so as not to cause casualties or material losses. One way to increase stiffness and structural resistance to earthquakes is to use shear walls [1]. Structural models with shear walls are considered more effective in resisting earthquake loads because displacement and force in structural elements are smaller than open frame structures [2]

One of the known methods of designing seismic-resistant buildings is the Force Based Design (FBD) method whose analysis procedures are found in SNI 1726: 2012 [3]. The Force Based Design (FBD) concept does not directly show the performance of the building against the effects of earthquakes. That is because in FBD analysis it is done linearly [4]. Along with the advancement of science and technology, it is known that a new performance-based concept that directly determines the performance of the structure is expected to be achieved when an earthquake occurs [5]. In this concept, one of the methods is Direct Displacement Based Design (DDBD) which uses the displacement value as a reference to determine the strength needed by the building on seismic forces[6] - [7].

In planning the structure of buildings, it is expected that the structures designed can be following the purpose and usefulness of a building[8]. For this reason, this study compares the performance of a dual system structure using the DDBD and FBD methods which aims to prove which methods have better performance with consideration of safety against users when an earthquake occurs.

2. METHODS

This study was conducted through modeling simulation as a 3D portal with software that was given load based on building loads data and seismic loads by the FBD and DDBD methods. The building functions as an office which consist of 10 floors located in Yogyakarta. Building a plan area of 700 m^2 and typical story height of 4 m as shown in **Figure 1.**

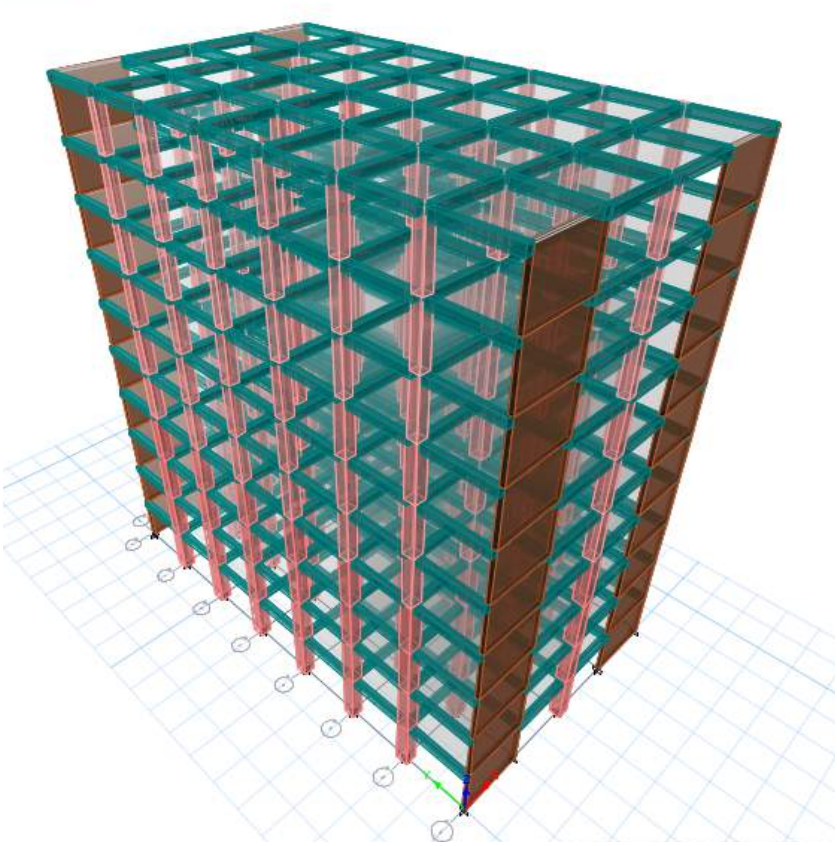

Figure 1. 3D Modeling of Dual System Structure

The method of study is focused on comparing the values of base shear, seismic loads distribution, reinforcement, and performance levels with the DDBD and FBD methods on dual system structures. Structural performance analysis used is static nonlinear pushover analysis. Flow chart the research method is illustrated in **Figure 2.**

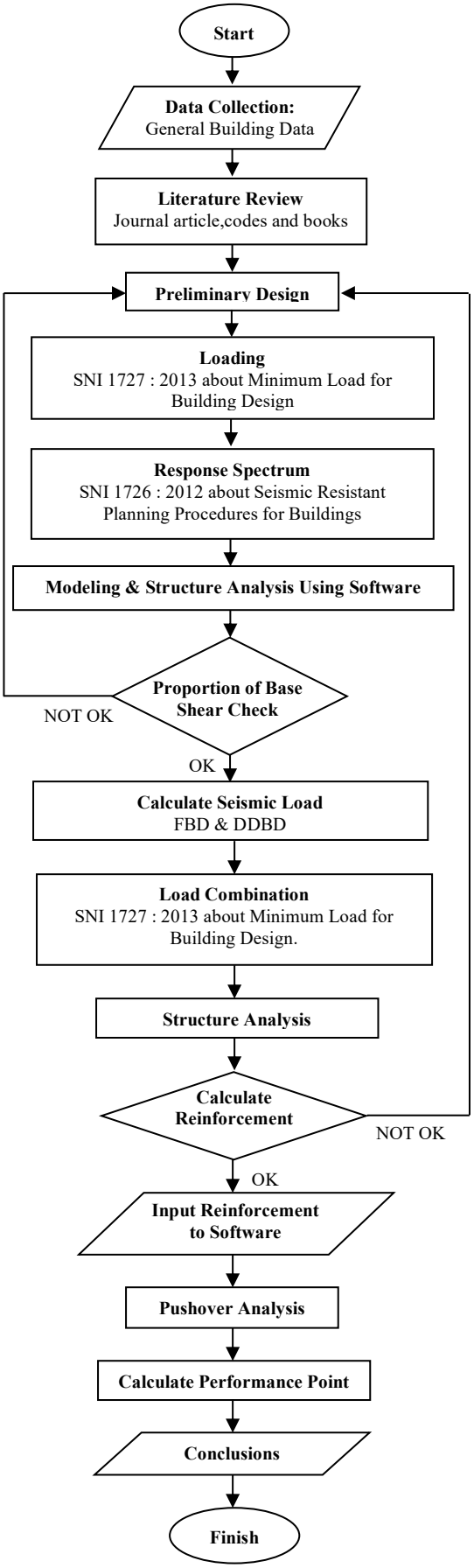

Figure 2. Flow Chart

3. RESULTS AND DISCUSSION

3.1 Base Shear Force

From the calculation of the base shear force with the DDBD and FBD methods, the value of the base shear force is obtained.

Table 1. Base Shear Force

Dir	Base Shear Force (kN)		% Base Shear Force to FBD	
	FBD	DDBD	FBD	DDBD
X	7992,34	6588,38	100,00	82,43
Y	7984,60	8733,19	100,00	109,38

Based on **Table. 1**, the value of base shear force x-direction in a structure designed using the DDBD method is 17.57% smaller than the value of the base shear force in structure designed using the FBD method. Whereas in the y-direction, the base shear force of the DDBD method is 9.38% greater than the base shear force of the FBD method**.**

3.2 Seismic Load Distribution

The distribution of seismic loads on each floor based on DDBD and FBD calculations is shown in **Figure 3.**

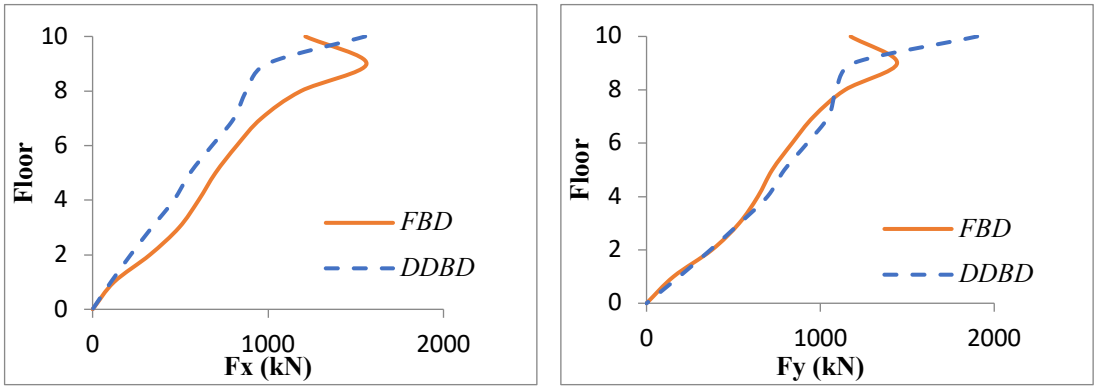

(a) Seismic Load Distribution Dir-X (b) Seismic Load Distribution Dir-Y

Figure 3. Seismic Load Distribution

Based on **Figure 3.**, the seismic load DDBD method value increases from floor 1 to floor 10. So that the most significant seismic load DDBD method is on the 10th floor, 1553,388 kN for the x-direction and 1901,57 kN for the y-direction. That is because, in the DDBD method, seismic loads are designed based on displacement of structural plans. So the seismic load value each floor increases to the top floor following the increase in design displacement. As for the FBD method, seismic load increases from floor 1 to floor nine then becomes smaller on the 10th floor. On the 9th floor, the value of seismic load in x-direction is 1561,329 kN and 1441,205 kN in y-direction. Then on the 10th floor, the value of the seismic load in x-direction becomes 1212,651 kN and in y-direction becomes 1173,847 kN. That is because, in the FBD method, seismic loads are designed based on building loads so that the seismic load on the 10th floor is smaller than the previous floor. Whereas in the DDBD method, seismic loads are designed based on displacement. The most significant design displacement is on the 10th floor, so the highest seismic load value is on the 10th floor [9].

3.3 Reinforcement ratio

Reinforcement requirements are calculated based on results of structural analysis using software with the FBD and DDBD methods, as shown below.

Table 2. Beam Reinforcement

Dir	As (mm^2)		The ratio of As to FBD	
	FBD	DDBD	FBD	DDBD
x - x	2551,76	2551,76	1,00	1,00
y - y	3118,82	3402,34	1,00	1,09

Based on **Table 2**. Percentage of beam reinforcement in y-direction DDBD method is 0.09% greater than the FBD method. The reinforcement area with FBD method is 3118.82 mm^2, and DDBD method is 3402.34 mm^2. Whereas in the x-direction, reinforcement area with the FBD and DDBD methods are same 2551.76 mm^2.

In the column structure element, the percentage of DDBD method reinforcement is also higher than the FBD method for columns K1, K2, and K3. The difference in the percentage of reinforcement column K1 in **Table 3**. is 0.09% with the area of reinforcement FBD method is 16725.84 mm^2, and DDBD method is 18246.37 mm^2. Column reinforcement K2 method FBD is 13684.78 mm^2, and DDBD method is 15205.31 mm^2 with a difference of 0.11%. Also, reinforcement of K3 column FBD method 10643.72 mm^2 and DDBD method 12164.25 mm^2 with a difference of 0.14%.

Table 3. Column Reinforcement

Type	Load	As (mm^2)	The ratio of As to FBD
K1 (1000 x 1000)	FBD	16725,84	1,00
	DDBD	18246,37	1,09
K2 (900 x 900)	FBD	13684,78	1,00
	DDBD	15205,31	1,11
K3 (800 x 800)	FBD	10643,72	1,00
	DDBD	12164,25	1,14

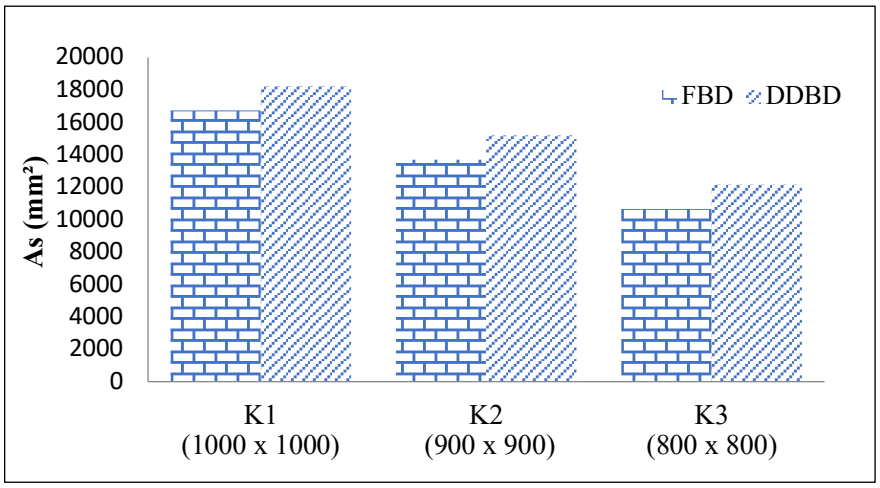

Figure 4. Diagram of Column Reinforcement

As for the shear wall reinforcement requirements, which are tabulated in **Table 4.** The DDBD method is 0.091% greater than the FBD method. The area of reinforcement by the FBD method is 21598,449 mm^2, and the DDBD method is 23561,945 mm^2.

Tabel 4. Shear Wall Reinforcement

Load	As (mm2)	The ratio of As to FBD
FBD	21598.449	1,000
DDBD	23561.945	1,091

Overall, the structural reinforcement with the DDBD method is more because, in its design, base shear force of the DDBD method is higher than the FBD method, so the moments that occur in the DDBD method structure planning are of greater value than the FBD method[10].

3.4 Structure Performance

Determination of the performance level of the dual system building structure by the FBD and DDBD methods is tabulated in **Table 5.**

Table 5. Performance Level

Dir	Parameter	Result of Pushover Analysis			
		FEMA -356		FEMA -440	
		FBD	DDBD	FBD	DDBD
x-x	Performance Point, Δm (m)	0,4167	0,4202	0,4387	0,4431
	Drift Actual (Δm/Ttot)	0,0104	0,0105	0,0110	0,0111
	Level (ATC – 40)	Damage Control	Damage Control	Damage Control	Damage Control
y-y	Performance Point, Δm (m)	0,5043	0,5184	0,4886	0,4906
	Drift Actual (Δm/Ttot)	0,0126	0,0130	0,0122	0,0123
	Level (ATC – 40)	Damage Control	Damage Control	Damage Control	Damage Control

Based on **Table 5.** it can be seen that each direction in the FEMA - 356 (displacement coefficient) method and FEMA - 440 (equivalent linearization) produces performance point value of FBD method as a whole at the level of damage control performance[11]-[12]. The performance level, according to ATC - 40, 1996 is a transition between Immediate Occupancy and Life Safety [13]. Buildings are still able to withstand earthquakes that occur with minimal risk of casualties[14].

For the performance level of DDBD method, the overall performance point value is also at the damage control. The value of the performance point has not yet reached the target level of design performance, namely life safety, but is at a safer level than the design level [15].

4. CONCLUSION

Based on the analysis and discussion in the previous, conclusions can be drawn, including:

1. The base shear force of the DDBD and FBD methods is close to the difference of 17.57% for the x-direction and 9.38% for the y-direction.
2. The reinforcement ratio of the DDBD method is more than the FBD method, with a small difference.
3. The difference between performance points between FBD and DDBD is minimal. Overall both are at the same level of performance, namely damage control so that the structure meets the building level performance requirements for offices.
4. Structural planning in this study for the same level of performance results, the DDBD method is more wasteful compared to the FBD method seen from the calculation of reinforcement needs.

5. ACKNOWLEDGEMENT

The authors would like to thank the P3M of Politeknik Negeri Jakarta for the fund provided by the BTAM program

6. REFERENCES

[1] Baehaki, Soelarso, and N. Fitria, "Analisis Perilaku Struktur Pada Sistem Ganda Apartemen 9 Lantai Menggunakan Metode Time History Analysis Sesuai Peraturan SNI 1726 : 2012," *J. Fondasi*, vol. 7, no. 1, 2018.

[2] A. H. Luih, K. Agusta, I. Muljati, and B. Lumantarna, "Evaluasi Kinerja Direct-Displacement Based Design Pada Perencanaan Bangunan Dengan Ketidakberaturan Tingkat Lunak," pp. 1–7, 2012.

[3] F. Perdana and Faimun, "Final Project (Rc14-1501) Application Of Direct Displacement Based Design For Dual System Building" 2015.

[4] E. Adel, Z. AbdelHamd, and E. Ahmed, "Comparison between Force Based Design and Direct Displacement Based Design for Reinforced Concrete Frame or Walled Structures," *Second Eur. Conf. Earthq. Enginering Seismol.*, 2014.

[5] N. Rianto and E. Leo, "Perencanaan Struktur Dengan Metode Ddbd Beserta Tingkat Kinerjanya Dan Idealisasinya Terhadap SNI 1726 : 2012," *J. Mirta Tek. Sipil*, vol. 1, no. 1, pp. 139–148, 2018.

[6] Tavio and U. Wijaya, *Desain Rekayasa Gempa Berbasis Kinerja (Performance Based Design)*, 2nd ed. Yogyakarta: ANDI, 2018.

[7] G. M. Calvi, M. J. N. Priestley, and M. J. Kowalsky, "Displacement-Based Seismic Design of Structures," 2007.

[8] S. Pangemanan and H. G. Mantiri, "Analisis Pushover Perilaku Seismik Struktur Bangunan Bertingkat : Studi Kasus Bangunan Ruko," *Pros. Simp. II*, vol. 40, no. September, pp. 978–979, 2017.

[9] R. Parulian Purba, Z. Djauhari, and R. Suryanita, "Kinerja Struktur Gedung Beraturan Dual System (Concrete Frame-Rc Wall Structures) Menggunakan Metode Direct Displacement Based Design Dan Capacity Spectrum Method," *Jom FTEKNIK*, vol. 3, no. 2, p. 1, 2016.

[10] F. Asisi, K. Willyanto, and I. Muljati, "Perbandingan Kinerja Bangunan Yang Didesain Dengan Force-Based Design Dan Direct Displacement-Based Design Menggunakan Sni Gempa 2012," *J. Dimens. Pratama Tek. Sipil*, vol. 4, no. 1, pp. 1–8, 2015.

[11] "Prestandard And Commentary For The Seismic Rehabilitation Of Buildings," *FEMA 356*, 2000.

[12] "Improvement Of Nonlinear Static Seismic Analysis Procedures," *FEMA 440*, 2005.

[13] ATC-40, *Seismic Evaluation and Retrofit of Concrete Buildings*. California, 1996.

[14] A. Y. Prakosa and A. Wibowo, "Desain Rekayasa Gempa Berbasis Kinerja Dengan Metode Direct Displacement Based Design (DDBD) (Performance Based Seismic Design using Direct-Displacement Method)," pp. 1–9, 2018.

[15] A. Alfianto, "Pemikul Momen Khusus Performance Based Design Dengan Pembebanan Gempa Menggunakan Sni 03-1726-20Xx Dan Beban."

LOGIC
Jurnal Rancang Bangun dan Teknologi
(Journal of Engineering Design and Technology)
Address : Gedung P3M, lt.1 Politeknik Negeri Bali, Bukit Jimbaran
PO BOX 1064 Kuta Selatan, Badung, Bali - Indonesia
Telp. (+62)361 701981 Fax. (+62)361 701128
Email: logic@pnb.ac.id